metals

MDPI

Review

Crystal Structure and Properties of Heusler Alloys: A Comprehensive Review

Asma Wederni *, Jason Daza, Wael Ben Mbarek, Joan Saurina, Lluisa Escoda and Joan-Josep Suñol *

Department of Physics, University of Girona, 17003 Girona, Spain; jason.daza@cadscrits.udg.edu (J.D.)
* Correspondence: asma.wederni@udg.edu (A.W.); joanjosep.sunyol@udg.edu (J.-J.S.)

Abstract: Heusler alloys, which were unintentionally discovered at the start of the 20th century, have become intriguing materials for many extraordinary functional applications in the 21st century, including smart devices, spintronics, magnetic refrigeration and the shape memory effect. With this review article, we would like to provide a comprehensive review on the recent progress in the development of Heusler alloys, especially Ni-Mn based ones, focusing on their structural crystallinity, order-disorder atoms, phase changes and magnetic ordering atoms. The characterization of the different structures of these types of materials is needed, where a detailed exploration of the crystal structure is presented, encompassing the influence of temperature and compositional variations on the exhibited phases. Hence, this class of materials, present at high temperatures, consist of an ordered austenite with a face-centered cubic (FCC) superlattice as an $L2_1$ structure, or body-centered cubic (BCC) unit cell as a B2 structure. However, a low-temperature martensite structure can be produced as an L10, 10M or 14M martensite structures. The crystal lattice structure is highly dependent on the specific elements comprising the alloy. Additionally, special emphasis is placed on phase transitions within Heusler alloys, including martensitic transformations ranging above, near or below room temperature and magnetic transitions. Therefore, divers' crystallographic defects can be presented in such types of materials affecting their structural and magnetic properties. Moreover, an important property of Heusler compounds, which is the ability to regulate the valence electron concentration through element substitution, is discussed. The possible challenges and remaining issues are briefly discussed.

Keywords: Heusler alloys; phase transition; crystal structure; thermal stability

Citation: Wederni, A.; Daza, J.; Ben Mbarek, W.; Saurina, J.; Escoda, L.; Suñol, J.-J. Crystal Structure and Properties of Heusler Alloys: A Comprehensive Review. *Metals* **2024**, *14*, 688. https://doi.org/10.3390/met14060688

Academic Editor: Ian Baker

Received: 10 April 2024
Revised: 6 June 2024
Accepted: 8 June 2024
Published: 10 June 2024

1. Introduction

Nowadays, the development of smart materials, materials that respond to an external stimulus by varying some of their properties or shape, have become more prevalent. These have been heightened with the technological advancements throughout many fields of knowledge. Shape memory alloys (SMA), which can be employed commonly in actuators, microcontrollers and sensors, can be positioned between the new functional materials [1]. The reversible phase shift from the low-symmetric, low-temperature martensitic phase to the high-symmetric, high-temperature austenitic phase, which can be altered by induced stress or induced temperature, is responsible for the shape recovery [2].

Owing to their unique comprehensive properties, such as the shape memory effect (SME), super elasticity (SE), biocompatibility, magnetic transformation, magneto caloric effect (MCE) [1] and high corrosion resistance, shape memory alloys (SMA) are widely used in various applications, such as aerospace components, magnetic sensors, biomedical implants, magnetic refrigeration and actuators [3,4]. The SME, which refers to a phenomenon in which pre-deformed materials can regain their original shapes after being heated [4], has gained a lot of attention as a key component of SMA over the years.

Because of their capacity to conduct reversible, solid-to-solid martensitic phase transitions, with adjustable shape change and energy conversion capabilities, shape memory alloys (SMA) are great candidates for solid-state actuation and thermal photovoltaic applications [5,6].

One of the most well-known types of smart alloys are the Heusler-type alloys. This category of materials possesses the aptitude to change and recover the original shape once exposed to strong magnetic fields. Consequently, these materials display a special attraction due to the magnetic response capacity to be faster and more forceful than responses brought on by the effect of temperature [7]. Some Heusler alloys demonstrate mutually ferromagnetic and shape memory properties at the same time, called magnetic shape memory alloys (MSMA). These effects can be tuned by both magnetic field and/or temperature [8]. These effects are attributed to a first-order martensitic transformation (FOMT) through a robust magneto-structural coupling in which a cubic high-temperature parent austenite phase transforms into a low-ordered martensitic phase by dropping the temperature [9]. The transformation temperatures in these types of alloys are determined by thermal analysis and/or vibrating sample magnetometer analysis.

Generally, magnetic shape memory alloys (MSMA) exhibit a large variation of magnetization during the martensitic transformation (MT), as in the transformation from the ferromagnetic (FM) austenite state into the paramagnetic (PM)/antiferromagnetic (AFM) martensite state [10]. There is constantly a significant coupling between the structural and magnetic configurations of the austenite and martensite phases [11]. Furthermore, the ferromagnetic (FM) to paramagnetic (PM) transformation can occur simultaneously with the structural transformation from austenite (AS) to martensite (MS). This magnetic change can occur in the austenite or martensitic zones, depending on the alloy and composition. Consequently, it is conceivable to combine AS-FM, AS-PM, MS-FM and MS-PM.

Within the most important systems, the typical Heusler Ni–Mn-based ferromagnetic shape memory alloys have received extensive attention during the past decades owing to their multifunctional properties [3]. It is worth noting that the MT temperature range and the magneto-structural properties are directly impacted by varying chemical compositions and multiple dopings in Heusler alloys. In this topic, numerous research studies have been conducted on the doping of quaternary element on off-stoichiometric Ni–Mn–Sn shape memory alloys, such as Ni–Mn–Sn–(Co, Cu, Fe) [12], Ni–Mn–Sn–Cu [13] and Ni–Mn–Sn–Pd [1]. With the addition of fourth-element atoms, we may tailor the transition temperatures (magnetic, structural) and the degree of hysteresis associated with the structural martensitic transition. In addition, MSMA are being investigated for their properties as half-metallic ferromagnets in the field of spintronics, thermoelectric and superconductors [14]. Hence, we aim to establish such alloys in order to enhance their physical characteristics and promote their application in the future.

It is important to note that Heusler materials date back to 1903, according to their history [15]. They first attracted the magnetism community's attention when Fritz Heusler was able to determine that a mixture of materials with the Cu_2MnAl chemical formula behaved as a ferromagnetic material despite the fact that it was composed of non-magnetic elements. Therefore, pure Mn exhibits an antiferromagnetic order. Because of the way that the atoms are arranged between them, a ferromagnetic behavior can be achieved. In other words, the magnetic properties of Heusler's are highly reliant by their crystalline structure. Hence, Heusler compounds present ternary intermetallic with a 2:1:1 stoichiometry, with X_2YZ being the general chemical formula [16].

Regarding the crystalline structure of full-Heusler compounds, they preferably crystallize in the cubic Cu_2MnAl structure with a Fm-3m space group, known as $L2_1$ cubic structure [17].

As the $L2_1$ phase presents the most ordered structure, the misplacing or arbitrarily occupation of X and/or Y atoms in the unit cell will disturb the phase order. Subsequently, this leads to the creation of disordered phases. Crystalline phases, such as the partially disordered B2 and D03 phases and the completely disordered A2 phase, can appear. The

B2 phase can be formed by the random distribution of Y and Z atoms' positions. However, the exchange of X and Y atoms in the unit cell results in the formation of the D03 structure. Nevertheless, the totally disordered A2 phase occurs when all atoms occupy positions randomly in the unit cell. Although, when one of the tetrahedral sites is vacant, it leads to the XYZ-type half-Heusler compound with C1b cubic structure. Researchers are drawn to the half-metallic ferromagnetic properties in Heusler alloys because of their potential spintronic application. Also, electronic band structure calculations have predicted 100% spin polarization for several full- and half-Heusler alloys [18].

As mentioned above, austenite is presented as the high-temperature, cubic phase of MSMA, while martensite is the low-temperature, non-cubic phase. The transformation from austenite to martensite occurs upon cooling the material below a critical temperature, known as the (MT), while the transformation from martensite to austenite occurs upon heating the material above a critical temperature, known as the (AT).

Indeed, when the material is cooled below the (MT) in the presence of a magnetic field, the martensite phase will be magnetically oriented, resulting in a magnetic shape memory effect. Similarly, the austenite phase will be magnetically oriented when the material is heated above the austenite transformation temperature in the presence of a magnetic field. This results in the magnetic shape memory effect. Undoubtedly, these phase transformations between austenite and martensite states are accompanied by a change in crystal structure. Martensite, on the other hand, as a non-cubic crystal structure, can present several different structures depending on the specific alloy and processing conditions [19]. The less symmetrical martensite phase can manifest a tetragonal, monoclinic or orthorhombic structure [16]. The martensitic domains shift and facilitate the creation of significant macroscopic deformations in the sample. In fact, martensite can be monitored (atomic sites deviate in a relatively periodic way) [20]. The displacement in this instance is caused by domain barriers, but the crystalline structure remains intact. Consequently, this deformation, also identified as a non-diffusional solid-state phase transformation, requires a relatively little amount of energy and is a reversible transition with low hysteresis and an insignificant volume modification [13]. In all martensitic structures, the unit cell is elongated along one axis compared to the other two axes. This transformation can result in significant changes in the physical properties of the material, including a change in shape and size, as well as changes in magnetic, electrical and mechanical properties. Hence, the lattice parameter of the unit cell of austenite is larger than that of martensite. In addition, the phase transformation involves a reversal of this distortion and reordering of atoms, resulting in the recovery of the original austenite structure. This transformation can also be accompanied by changes in physical properties [21]. Understanding the structural changes that occur during the phase transformations between austenite and martensite is important for designing and optimizing MSMA for specific applications. In this review, we scrutinize the impact of Cu and Pd doping on structural variations and magnetic properties of Heusler Ni-Mn-Sn magnetic shape memory alloys in various combinations.

2. Classification of Heusler Alloys

Full-Heusler, half-Heusler and inverse-Heusler alloys are the three categories for ternary Heusler alloys. Furthermore, binary and quaternary compounds are formed from Heusler alloys as a result of structural changes and chemical substitutions.

The conventional formula for full-Heusler alloys is X_2YZ (2:1:1), where Z atoms are part of the main group (III or IV) of the periodic table, and X and Y atoms are transition metals or lanthanides [22].

2.1. Symmetric Heusler Alloys

2.1.1. Conventional Heusler Alloys

Conventional Heusler alloys are formed by transition metals (d-metals) and the main group (p-group), which is presented by Z atoms (D sites). These alloys typically present the X_2YZ composition, where X and Y are transition metals, and Z is a main-group element and often crystallizes in the face-centered cubic (FCC) structure. Moreover, the p-d hybridization present in conventional Heusler alloys significantly affects the parent phase's stability, atomic ordering and magnetic response [23]. However, the d-d hybridization influences the martensite transformation, as stated by Roy et al. [24]. The periodic table of each element that comprises the full-Heusler alloys is illustrated in Figure 1. Regularly, the first chemical element in the formula is the transition metal, whereas the main group atom is placed at the end, such as Co_2MnGe and Co_2MnSi [25,26]. Nonetheless, this rule does not apply to compounds like Li_2CuSb, where one of the elements is defined as the most electropositive. According to IUPAC criteria, the most electropositive element is the first component in the formula. As aforementioned, full-Heusler alloys display an $L2_1$ cubic structure and belong to the Fm-3m space group. However, full-Heusler alloys may demonstrate A2 (X-Y-Z disorder) and B2 (Y-Z disorder) structures, depending on the site-disordered state. Otto Heusler [15] originally established the basic structure for Cu_2MnAl, and Meyers et al. for Cu_2MnSn [27]. In full-Heusler alloys system, four interpenetrating FCC sublattices constitute the cubic unit cell, where atoms are situated following Wyckoff positions. X atoms are placed at the 8c (1/4, 1/4, 1/4) position of the unit cell, and four Y and Z atoms are placed at the 4a (0, 0, 0) and 4b (1/2, 1/2, 1/2) positions, respectively, as proved by Otto Heusler [15]. According to Graf et al. [28], this structure, which was created by a single X and Z atomm is referred to as a zinc blende sublattice. Furthermore, a Y atom is positioned in the octahedral sites, and the second X atom is in the tetrahedral sites [22].

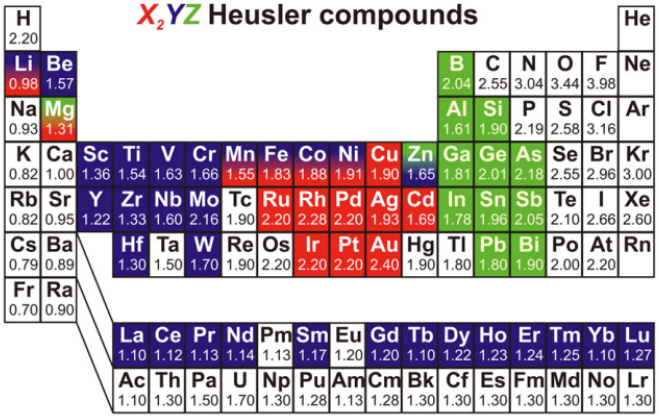

Figure 1. Periodic table of the elements. The huge number of Heusler materials can be formed by a combination of the different elements according to the color scheme (reprinted with permission from Ref. [29]).

2.1.2. All D-Metal Heusler Alloys

On the other hand, however, all-d-metal Heusler alloys are formed exclusively by transition metals, which means the Z atoms are also a transition metal (D sites) [29]. The distinguishing feature of all-d-metal Heusler alloys is the absence of main-group elements in their composition. They have a specific composition where all the elements (X, Y and Z) belong to transition metals. These alloys are characterized by having all-d-electron configurations in their constituents. The two types of alloys may present diverse crystal structures as a result of this compositional difference. Accordingly, the crystal structure of all-d-metal Heusler alloys can differ and depends on the specific elements involved. They

may favor different structures as non-FCC structures. Otherwise, they might not necessarily follow the cubic symmetry present in conventional Heusler alloys [30]. The differences in hybridization and chemical elements between conventional and all-d-metal Heusler alloys are shown in Figure 2 [29].

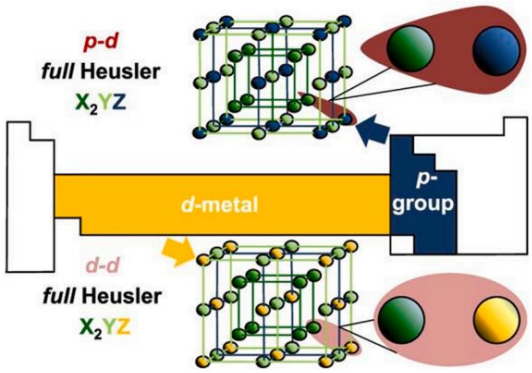

Figure 2. Difference in hybridization and chemical elements between conventional and all-d-metal Heusler alloys (reprinted with permission from Ref. [29]).

2.1.3. Half Heusler Alloys

Half-Heusler alloys are presented by the following chemical formula XYZ (1:1:1). These compounds show covalent and ionic parts, where X and Y elements possess cationic character, though Z displays the anionic character. The X element is the most electropositive element, forming a rock-salt (NaCl) sublattice with the main-group atom Z. This interaction corresponds to a stronger ionic character of their bonding [29]. The Y and Z atoms form a zinc-blend (ZnS) sublattice; this indicates covalent bonding [31]. Accordingly, the sum of zinc-blend and rock-salt lattice forms the structure of half Heusler alloys [29]. Figure 3 illustrates the difference between a full- and half-Heusler compound. These alloys crystallize in a C1b cubic structure, belonging to the F43m space group [32]. Filling the vacancies in the octahedral lattice sites in the tetrahedral ZnS structure yields half-Heusler alloys, which have a non-centrosymmetric arrangement and constitute a ternary ordered modification of the CaF_2 structure [33]. As stated by certain authors, four FCC sublattices might additionally be employed to represent these compounds while one sublattice is empty [34]. In this situation, X atoms are situated in Wyckoff positions 4c (1/4, 1/4, 1/4), Y atoms are located in the 4b (1/2, 1/2, 1/2) positions and Z atoms occupy the 4a (0,0,0) position, respectively. Furthermore, Table 1, expresses that for such a type of structure, three distinct atomic combinations are conceivable [14].

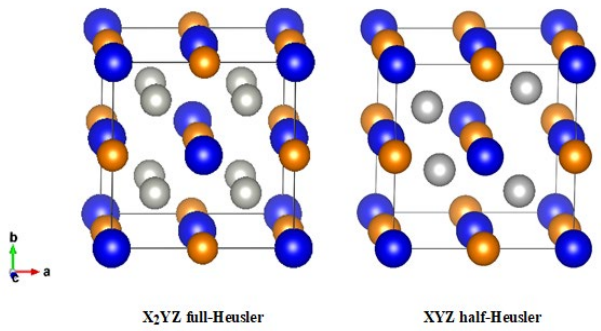

Figure 3. Crystal structure of full- and half-Heusler compounds (X atoms occupy the gray positions, Y atoms occupy the orange positions and Z atoms occupy the blue positions).

Table 1. Different site occupancies in C1b-type structure. Atoms located on 4a and 4c Wyckoff positions form a ZnS sublattice, while the 4b atoms are placed on the octahedral sites (reprinted with permission from Ref. [33]).

Type	4a	4b	4c
I	X	Y	Z
II	Z	X	Y
III	Y	Z	X

2.2. Less Symmetric Heusler Alloys

2.2.1. Inverse Heusler Alloys

Inverse-Heusler alloys are derived from full=Heusler alloys through a rearrangement of the atomic positions. Compared to the X_2YZ formula of full-Heusler alloys, in inverse-Heusler alloys, the positions of X and Y are interchanged, leading to a different crystal structure. This inversion of the X and Y positions alters the electronic and magnetic properties of the material. Commonly, the site preference of the metal transition atoms depends on the number of valence electrons (ZV). In other words, if ZV(Y) > ZV(X), where X and Y are transition metal elements belonging to the same period of the periodic table, two X atoms occupy two sites, precisely (½, ½, ½) and (¾, ¾, ¾), whereas Y and Z atoms are located in the remaining positions, (¼, ¼, ¼) and (0, 0, 0), respectively, resulting in the XA type structure with F43m space group [14]. Referring to Graf et al., to better understand the XA crystal structure, X and Z atoms form a NaCl structure in order to reach an octahedral arrangement for X [28]. However, X and Y elements fill up the tetrahedral interstitial sites [35]. The difference between the full- and the inverse-Heusler alloys' crystal structure is presented in Figure 4.

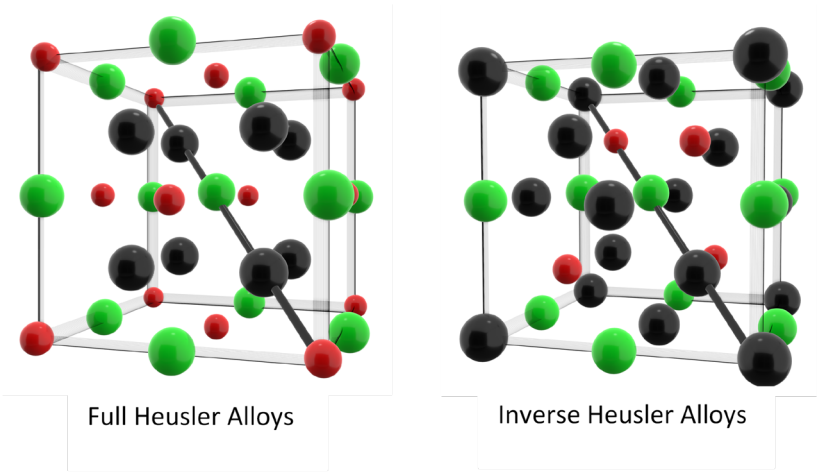

Figure 4. Comparison between regular full- and inverse-Heusler crystal structure (X atoms occupy the black positions, Y atoms occupy the green positions and Z atoms occupy the red positions).

2.2.2. Binary Heusler Alloys

Binary Heusler alloys can display the X_3Z (3:1) chemical formula, with X being the transition metals and Z elements of the main group [36]. These alloys present a face-centered cubic structure D03-type and present the same space group Fm-3m of full Heusler alloys. When the X and Y elements of full-Heusler compounds are the same chemical element, a D03-type structure is formed. Therefore, three X1, X2 and X3 atoms are positioned in the (¼, ¼, ¼), (½, ½, ½) and (¾, ¾, ¾) sites, and Z atoms fill up the (0, 0, 0) positions. This arrangement leads to a ferromagnetic interaction between the two X1, X3 and X2 atoms, as the positions occupied by X1 and X3 are equivalent [37]. Figure 5 presents the D03-type crystal structure.

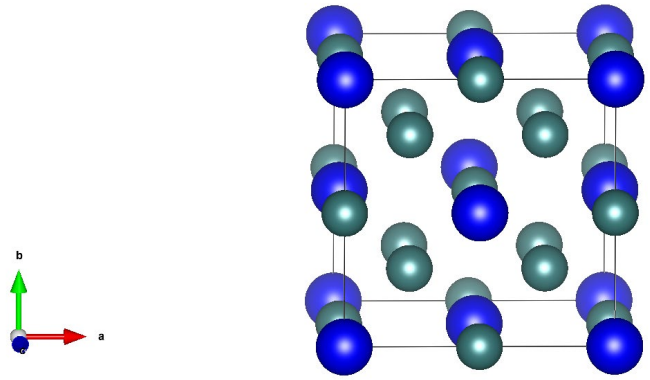

Figure 5. Binary X_3Z Heusler structure (X atoms occupy the green positions, and Z atoms occupy the blue positions).

2.2.3. Quaternary Heusler Alloys

Quaternary Heusler alloys are a type of Heusler alloys exemplified by an LiMgPdSn-type crystal structure (known as Y-type structure), whose primitive cell contains four atoms. Likewise, these types of alloys follow the same symmetry as half and inverse Heusler with an F43m space group [38]. Depending on the atom positions, three nonequivalent structures are obtained for the Y-type arrangement. Table 2 presents three different atom arrangements, mentioned as type 1, type 2 and type 3 at various Wyckoff positions [38]. The chemical formula XX′YZ is demonstrated in the quaternary Heusler compounds due to the stability along the FCC cube's diagonal. Rather than being formed by a single element, X and X′ are formed by distinct chemical elements. The valence of the elements in these types of alloys is another characteristic; X atoms have a higher valence than X′, while Y atoms have a lower valence than both X and X′ elements [14]. Three-unit cell structures with the possible arrangement sites of the quaternary Heusler are represented in Figure 6 [38].

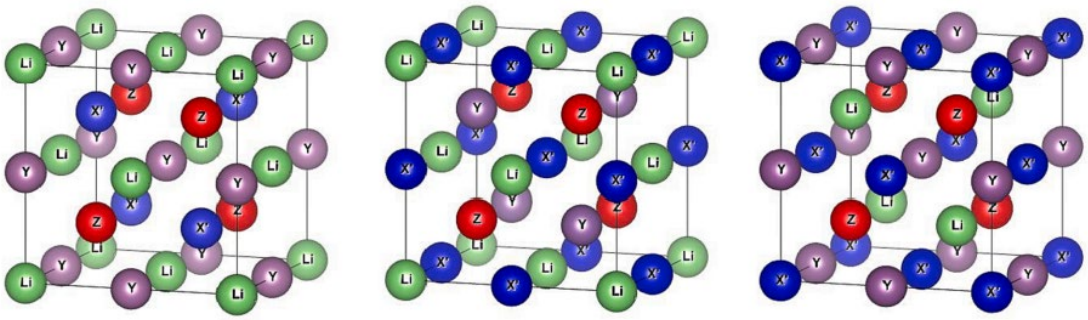

Figure 6. Unit cells representation of quaternary Heusler Li (X)X′YZ; type Y1, type Y2 and type Y3 (reprinted with the permission from Ref. [38]).

Table 2. Different types of structures for quaternary Heusler alloys with Wyckoff positions (reprinted with the permission from Ref. [38]).

Type	4a	4c	4b	4d
Y1	X	X′	Y	Z
Y2	X	Y	X′	Z
Y3	X′	X	Y	Z

2.2.4. Non-Stoichiometric Heusler Alloys

Based on stoichiometry, the Heusler alloys are classified as described above. On the other hand, many Heusler compounds present non-stoichiometric compositions. Non-stoichiometry can arise due to a range of factors, including defects in the crystal lattice, substitutions, vacancies or compositional variations within the material. These deviations from stoichiometry can have significant impact on the alloy's physical, chemical and electrical properties. In such circumstances, the crystal's chemical order may shift from the totally ordered $L2_1$ structure to a partially ordered B2 within an exchange of atoms on the Y and Z sites positions or to a fully disordered A2 structure, where all the elements, X, Y and Z, are randomly distributed [25,26]. As a result, the distance between the magnetic atoms may also change, altering the exchange interaction between chemical elements [23].

2.2.5. Atomic Disorder in Heusler Alloys

Furthermore, the complicated crystallographic structure, $L2_1$, which consists of four interpenetrating face-centered cubic cells and where the atomic order affects the properties, is responsible for all of the Heusler alloys characteristics [39]. The ordered structures provide the best features, although a disordered structure can also occur. The most prevalent kind of disorder is associated to the random switching of the Y and Z atoms, resulting in a lower symmetry phase and a B2-type structure, which is a primitive unit cell rather than the FCC cell (Fm-3m→Pm-3m) [26,40], as shown in Figure 7 [40].

From theoretical calculations, it is important to note that the B2-type disorder structure generated in Y–Z elements affects the spin polarization values considerably less than the X–Y and X–Y–Z disorders, which both significantly reduce this feature [41]. As a result, one of the primary difficulties in producing X_2YZ full-Heusler alloys is obtaining the good properties of the chemically ordered $L2_1$ phase. Moreover, according to ab initio calculations [42] and experimental observations [43], the physical characteristics (cell parameter, Curie temperature, magnetic moment and spin polarization) of the $L2_1$ and B2 phases are somewhat distinct from one another, and the half-metallic spin gap should be preserved. In addition, Heusler alloys, on the other hand, can crystallize in different phases with reduced chemical ordering, without altering the atomic sites in the lattice [44]. Moreover, the p-d hybrid state that occurs in the typical Heusler alloys is thought to be crucial for both the structural instability that causes the martensitic phase change and for stabilizing the Heusler structure [39]. However, all-d-metal systems do not provide any additional p-electrons. Accordingly, a d-d hybridization must assume this role [45]. Meanwhile, a stable structure can be achieved for every Heusler alloy. It is plausible that the distinct hybridization occurring in the all-d-metal Heusler alloys also influences the ordering arrangement [44]. Several authors have attested that Co-containing Heusler alloys are sensitive to chemical disorder by a drastic shift of the phase transition, owing to a change of magnetic interactions between atoms [44]. Likewise, it is evidenced that the existence of the B2 disorder structure strongly affects the magnetic and coercivity behaviors at applied low magnetic fields [26]. Thus, theoretical X-ray diffraction (XRD) patterns of Co_2MnSi were simulated for different crystal structures, with $L2_1$, B2, DO_3 and A2 being displayed in Figure 8. In order to determine the degree of B2 and $L2_1$ ordering in the alloys, the following equations were used:

$$(I200/I220)\ \mathrm{exp} = SB2^2 (I200/I220)\mathrm{th} \quad (1)$$

$$(I111/I220)\ \mathrm{exp} = [SL2_1\ (3 - SB2/2)]2\ (I111/I220)\mathrm{th} \quad (2)$$

where I (hkl) denotes the Bragg peak's intensity Miller indices (hkl), the suffix 'exp' signifies the experimentally obtained intensities values and 'th' represents the theoretically simulated ones, respectively [46]. The degree of B2 and $L2_1$ ordering is represented by SB2 and $SL2_1$, respectively [26].

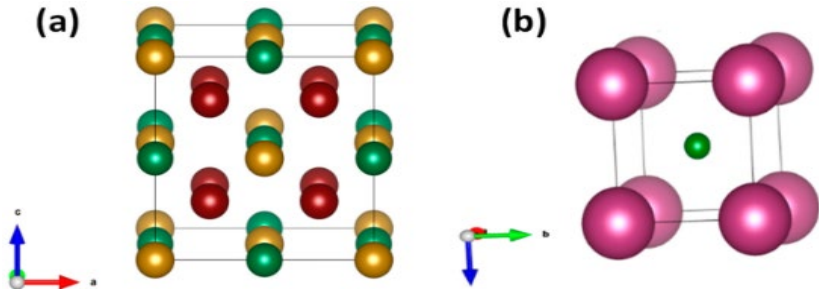

Figure 7. (**a**) $L2_1$ cubic structure; (**b**) B2 cubic structure [26]. Each color represent an atomic site of the structure.

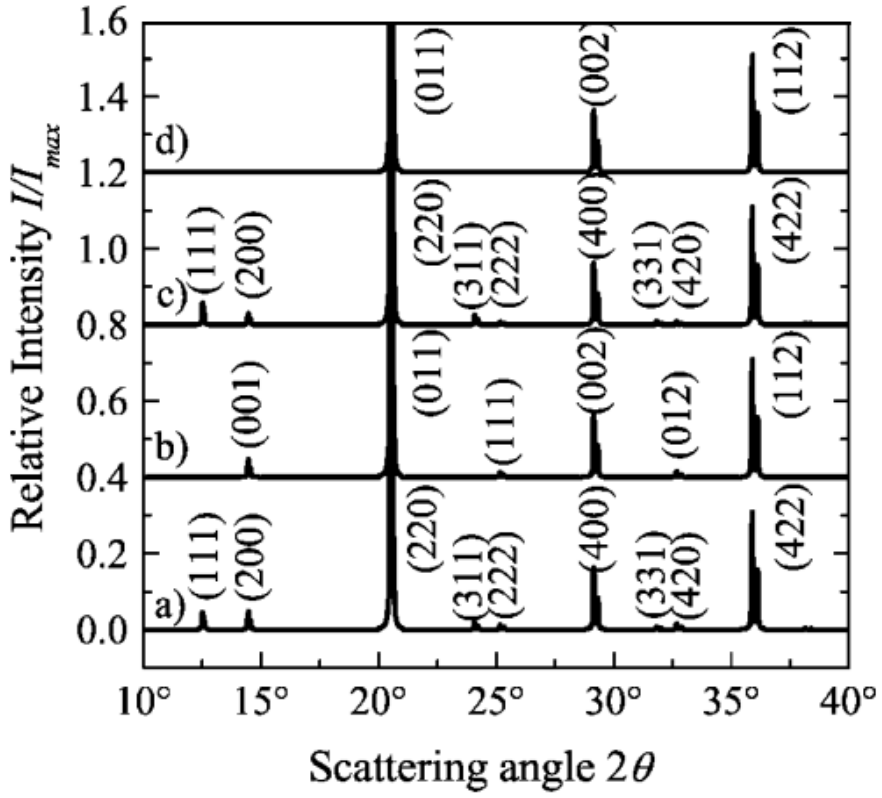

Figure 8. Simulated X-ray diffraction patterns measured with Mo-Kα radiation for Co_2MnSi in different crystal structures: **a**) Cu_2MnAl-type ($L2_1$), **b**) CsCl-type (B2), **c**) BiF_3-type (DO3), **d**) tungsten-type (A2) (reprinted with the permission from Ref. [14]).

2.2.6. Crystallographic Defects in Heusler Alloys

Produced Heusler alloys are frequently exposed to several kinds of point defects and lattice distortions. These crystal defects can be minimized or exploited based on the desired material properties; they can affect the properties and performance of Heusler alloys.

In this context, Qiu et al. [47] studied the changing antisite defects' degree in ZrNiSn Heusler alloys and found that it can improve the thermoelectric performance of this alloy, where the antisite of Zr and Sn atoms can modify the band structure and influence the electrical transport properties performance greatly. Likewise, Jodin et al. [48], confirmed the improvement of the thermoelectric performance in FeVSb half-Heusler alloys through an excess of Sb (or vacancies on the Fe sublattice) as well as the disorder between V and Sb. Other studies on the Co_2MnAl alloys have reported some exceptional properties, where various point defects (such as binary antisite disorder, ternary antisite disorder and vacancy defects) and the lattice distortions (uniform cubic strains and tetragonal distortions) affect the structural, electronic and magnetic properties [49]. They have found that

the disordered structures maintain the high spin polarization (≥70%) and nearly same magnetization as that in the $L2_1$-ordered structure. Furthermore, the tetragonal Heusler alloys can be considered as tetragonal distortions from the cubic structure along the z direction, and the c/a ratio can be used to quantify the amount of tetragonal distortion [50]. The elongation along the c-axis (with compression of the ab-plane) is the favored condition for the occurrence of tetragonal distortion than compression along the c-axis (with elongation of the ab plane) [49]. For tetragonal X_3Z (Z = Al, Ga, In Tl, Si, Ge, Sn, Pb) alloys, the X(A), X(B), X(C) and Z atoms occupy the (0, 0, 0), (0.25, 0.25, 0.25), (0.5, 0.5, 0.5) and (0.75, 0.75, 0.75) Wyckoff positions, respectively [22]. Thus, Chen et al. [51] detected metastable tetragonal phase formation in Mn_2CoAl upon Ar+ irradiation. They found that the saturation magnetization decreased, and an anomalous Hall resistivity progressively deviation from negative to positive was observed as a result of the structural deterioration.

3. Characteristics and Properties of Heusler Ni-Mn-Sn-X Alloys

The magneto-structural transition in Ni-Mn-Sn Heusler magnetic shape memory alloys (MSMA) refers to a phenomenon where a change in the magnetic state of the material leads to a structural transition in the crystal lattice. Instead of the Ni-Mn-Ga alloy, recent research has focused on the new MSMA of the Ni-Mn-Sn alloys with and without substituting the fourth element [10,12,52–55].

3.1. Structure and Phase Change in Ni-Mn-Sn-X Heusler Alloys

The structure of Ni-Mn-Sn MSMA depends on its temperature. Thus, the phase change in Ni-Mn-Sn MSMA occurs due to a shift in the relative stability of the austenitic and martensitic phases as the temperature changes. It is important to note that at high temperatures, the austenitic phase is stable, whereas the martensitic phase is stable at low temperatures. Likewise, the shape change in Ni-Mn-Sn MSMA ensues due to the rearrangement of the crystal structure during the phase transformation. As the material transforms from the austenitic to the martensitic phase, it undergoes a change in shape, which is reversible upon returning to the austenitic phase. In this context, XRD is a non-destructive technique used to analyze the crystal structure and phase composition of materials, where diffraction patterns can provide us information about the arrangement of atoms and, consequently, the crystallographic structure and atoms positions [46]. The XRD experiments are typically performed using a diffractometer equipped with an X-ray source (e.g., Cu Kα radiation). The diffraction patterns are recorded, and the intensity of diffracted X-rays is measured at room temperature, although elevated temperatures can also be employed for studying phase transformations in some case [27]. The magneto-structural evolution of Heusler Ni-Mn-Sn alloys was studied by Hernando et al. [56]. They demonstrated that the alloys were monophasic, and the high-temperature parent phase was ferromagnetic $L2_1$ austenite. Moreover, at low temperatures, the austenite phase was transformed into a martensite phase with an orthorhombic 7 M, monoclinic 10 M and monoclinic 14 M symmetry-modulated structure.

Similarly, Chabri et al. reported that the $Ni_{45}Mn_{44}Sn_{11}$ alloy was confirmed to be in cubic $L2_1$ austenitic phase with lattice parameter a = 5.945 Å at room temperature [57]. Referring to the $L2_1$-order degree, the development of the intensities of super lattice reflection peaks like (111) and (311) allows one to estimate it qualitatively. In addition, in the abovementioned study, the authors validated the first-order martensite transition extracted from the large exothermic and endothermic peaks found in the calorimetric measurements [58]. The structural modification was equally investigated by Krenke et al. in Ni-Mn-Sn MSMA [59]. On the basis of Sn composition, they proved that the austenite structure was of the $L2_1$-ordered type, whereas the martensite was of the 10 M, 14 M, or L10 type. Similarly, they concluded that both phases exhibited ferromagnetic behavior. Studies performed by Bachaga et al. [8] have examined $Mn_{50}Ni_{50-x}Sn_x$ SMA and have determined that the martensitic phase resulting in a phase transformation from austenite is a 14 M-modulated monoclinic structure. Other authors have stated that the $Ni_{1.9375}Mn_{1.5625}$

$Sn_{0.5}$ discloses a four-layer-modulated 4O structure with Mn excess atoms randomly distributed in the Ni and Sn sublattices [60]. Wang et al. indicated that the stoichiometric Ni_2MnSn alloy does not undergo a martensitic phase transition from the cubic Heusler $L2_1$ structure to the non-modulated structure [61], whereas studies on the $Ni_2Mn_{1+x}Sn_{1+x}$ alloys have demonstrated that the martensitic transition can only be seen in Mn-rich conditions with $x \geq 2$ [55].

$Mn_{50}Ni_{50-x}Sn_x$ (x = 7–10) MSMA structural modification was researched by Yiwen et al. [62]. It was shown that the increase of Sn content resulted in a decrease of martensitic transformation temperatures in the ribbons. Due to the strong magneto-structural coupling in $Mn_{50}Ni_{40}Sn_{10}$ MSMA ribbons, the field-induced reverse martensitic transformation from a weak magnetic martensite to a ferromagnetic austenite was established. The results specify that at room temperature, ribbons with Sn contents of 7% and 8% exclusively showed a single martensite phase. Once the Sn concentration was raised to 9%, supplementary austenite diffraction peaks were apparent in the XRD pattern in addition to the martensite peaks, proving that the ribbons are composed of both phases at room temperature.

Afterwards, the structural phase completely changed into a single austenite with a cubic $L2_1$ structure when the Sn concentration reached 10%. Hence, an increase in Sn content tends to make austenite more stable.

Numerous studies have discussed the substitution of fourth elements on Ni-Mn-Sn compositions such as Wederni et al. [46], who investigated the influence of Cu doping on $Ni_{50-x}Mn_{36}Sn_{14-y}Cu_{x,y}$ (x = 0, 1, 2 and y = 1 at. %). They stated that the addition of Cu, with the corresponding reduction of Ni, stabilized the austenite phase and increased the martensitic start temperature from 194 to 228 K, whereas replacing small amounts of Cu for Sn stabilized the modulated martensite phase and increased the martensitic transformation temperature from 194 to 325 K. As the Cu content rises, the transformation temperatures often rise as well.

It was recognized from other studies [63] that the austenite phase with the $L2_1$-type structure was designed in $Ni_{50-x}Cu_xMn_{38}Sn_{12}$ (Fm-3m space group) with a lattice parameter of a = 0.5967 nm, 0.5970 nm, 0.5973 nm and 0.5976 nm for x = 0, 1, 2 and 5, respectively. A regular rise in the lattice parameter was seen when Cu was substituted for Ni. This could be related to the differing ionic radius sizes of Ni and Cu. Because of the high rate of the Cu substitution, an obvious shift from martensite transition temperature to low temperatures was clearly observed. If we assume that Cu^{2+} atoms occupy exactly Ni^{2+} sites, then the larger ionic radius of Cu^{2+} (0.128 nm) compared to Ni^{2+} (0.125 nm) would result in an increase of the lattice parameter.

It has been shown that the substitution of Ni by Cu and Co in $Ni_{46-x}Mn_{43}Sn_{11}$[64] results in a shift of the martensitic transition to a lower temperature, while the transition shifts to higher temperatures when Cu doping atoms replaces Sn in the off-stoichiometric $Ni_8Mn_6Sn_2$ [55]. It is worth pointing out that the simulated structure in this case is ordered; however, in a real material, the distribution of the Cu and Mn ions on the Sn sites would be random.

Additionally, Wederni et al. analyzed and investigated the effect of Pd substitution on the Ni-Mn-Sn-Pd alloys [13]. They revealed that the martensitic transition and magnetic characteristics are sensitive to the Palladium concentration, even in small amounts. Thus, the substitution of Pd on Ni sites express a $L2_1$ austenitic state (X sites of the Heusler structure), and a modulated monoclinic martensitic structure by the substitution of Pd on Sn sites (Z sites). Otherwise, the structural transition temperatures rise if Pd atom sites substitute Ni or Sn sites and the cell parameters shift equally to higher values. Likewise, in such an off-stoichiometric SMA, additional Mn atoms could occupy certain Sn positions. Therefore, along the (110) directions, Mn atoms can have Mn atoms as their nearest neighbors. At that point, the Mn-Mn interatomic distance became closer than that of the stoichiometric composition.

Generally, the alloys' crystal structure is examined in relation to the magnetic properties, which include exchange interactions, magnetic moments and spin configurations [65].

Phase transitions in the X_2YZ-type alloys are linked to magnetic ordering. The discovery of critical magnetic transitions, including ferromagnetic to antiferromagnetic and paramagnetic states, emphasizes how crystallographic variations affect the magnetic behavior [66]. As reported in earlier studies, the excess of Mn atoms in the Ni_2MnSn alloys prefers to occupy the Sn sites. In Figure 9, Mn atoms at Mn sites are marked as Mn-Mn, while Mn atoms that substitute Sn atoms in the Sn sites from stoichiometrically Ni_2MnSn alloy are marked as Mn-Sn. Moreover, two situations of magnetic moments are considered. Hereafter, "AP" represents the antiparallel magnetic interactions between the Mn-Mn and Mn-Sn, and "P" represents their parallel magnetic interactions [67].

Thus, as detailed by Xu et al. [66], the ferromagnetic coupling between NiX/CoX and MnY ions and the antiferromagnetic coupling between NiX/CoX and MnZ ions can be used to represent the magnetic ordering of the X_2YZ-type in $(Ni_{1-x}Co_x)_2MnGe$ Heusler alloys.

Furthermore, the identification of magnetic moments in half- and full-Heusler alloys was conducted in other studies [68], describing that XYZ half-Heusler compounds can display only one magnetic sublattice since only the X atoms on the octahedral sites convey a local magnetic moment. However, X_2YZ Heusler alloys present two magnetic sublattices, which can be coupled ferromagnetically or antiferromagnetically.

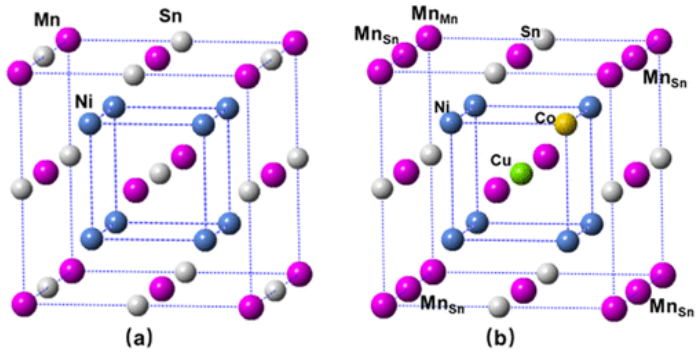

Figure 9. Unit cell of the cubic structure of (**a**) Ni_2MnSn and (**b**) NiCoMnSnCu alloys (reprinted with the permission from Ref. [67]).

3.2. Thermal Properties in Heusler Alloys

Differential scanning calorimetry (DSC) is a process of thermal analysis that measures the enthalpy of phase transformation in a material that undergoes structural changes as a function of temperature and time, depending on whether heat is released or absorbed. Heusler materials, and more precisely MSMA, represent a distinctive class of metallic materials characterized by their remarkable ability to undergo reversible solid-to-solid transformations, resulting in substantial recoverable strains upon exposure to controlled temperature changes. The investigation of thermal stability and phase transitions within these materials requires a meticulous reliance on XRD analysis. The phenomenon of thermal hysteresis, a prominent feature observed during the martensitic transition, undergoes the inherently first-order nature of this phase change. To discern the martensite-austenite transition effectively, differential scanning calorimetry (DSC) scans can be conducted, entailing heating/cooling procedures from ambient temperature to temperatures surpassing the austenite start temperature, As. Conversely, DSC scans are executed through cooling/heating sequences from room temperature to temperatures below the martensite start temperature, Ms, to obtain an austenite-martensite transition. A thorough comprehension of these DSC thermal results holds a huge significance for optimizing the

functionality and reliability of these alloys across various practical applications [22]. It is frequently a crucial step in the characterization process and is used to determine the martensitic transition temperatures, heat flow curves, thermal hysteresis and enthalpy/entropy changes in shape-memory Heusler alloys [69]. As abovementioned, the calorimetric DSC studies were conducted in terms of heating followed by cooling cycles to determine the structural transition temperature (TM). A well-defined endothermic peak appearing during heating indicated the martensite to austenite phase transformation, while an exothermic peak was detected upon cooling, representing the austenite to martensite phase transformation [58]. The endothermic and exothermic peaks in the DSC thermograms, which characterize the martensite start and finish (Ms, M_f) and austenite start and finish (A_s, A_f) temperatures, respectively, were used to determine the typical transition temperatures, as illustrated in Figure 10. These are revealing of a first-order phase transition. The heat created with the production of martensite-austenite transitions is what causes the DSC curves to appear [1]. For example, in $Ni_{50-x}Mn_{37+x}Sn_{13}$ alloys, a decrease in the Ni/Mn ratio or an increase in the Mn content results in a decline in the martensitic transformation temperature [70]. In the study conducted by Wederni et al. [46], the authors acquired the typical transformation temperatures from differential scanning calorimetry scans. It was observed that the copper addition for Ni led to the stabilization of the austenite phase (increasing the martensitic start temperature from 194 to 228 K); however, substituting minor amounts of Cu for Sn stabilized the modulated martensitic phase (increasing martensitic transformation temperature from 194 to 325 K). Generally, the transformation temperatures rose by increasing the Cu content. Furthermore, with Te doping in $Ni_{43}Mn_{46}Sn_{11-x}Te_x$ Heusler compounds, the martensite transition temperature increased from 215 K to 289 K to be near room temperature [71].

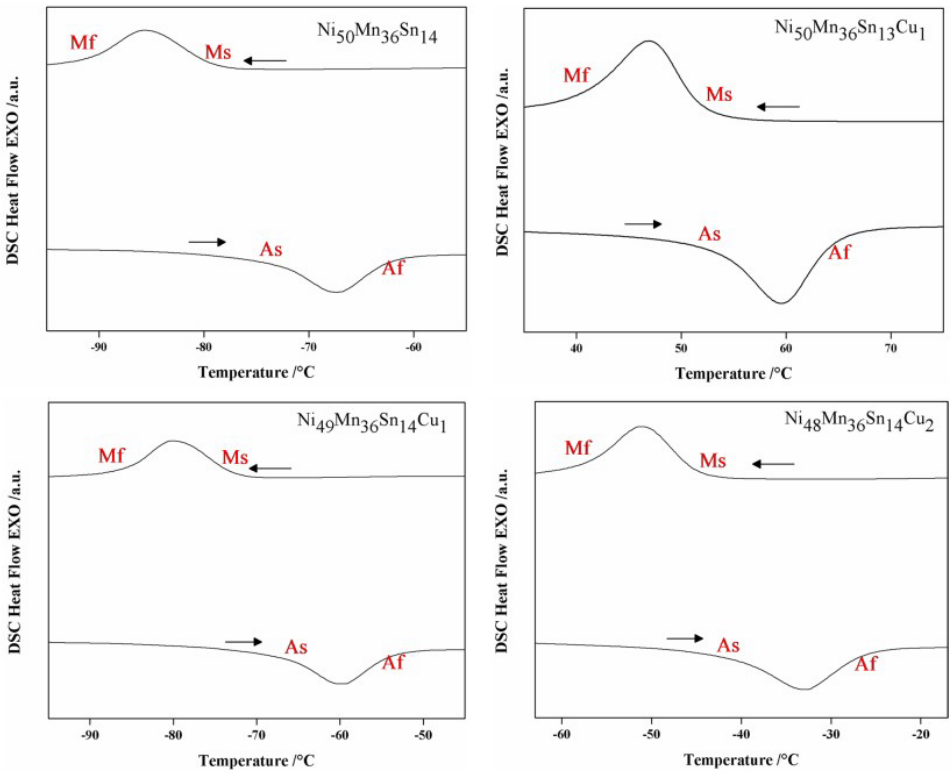

Figure 10. DSC curves during the heating and cooling processes. The reverse martensitic transition (austenitic transition) upon heating start (As) and finish (Af) temperatures and martensitic transition upon cooling start (Ms) and finish (Mf) temperatures are indicated (the arrows indicate the cooling or the heating process)(reprinted with the permission from Ref. [46]).

Mostly, the average number of valence electrons by atom (e/a) is a parameter that has a strong effect on the martensitic transition temperature in Ni-Mn-Sn Heusler alloys [46]. The e/a ratio is calculated as the concentration-weighted average of the valence (s, p and d) by extracting the electron configurations from the outer shells of various elements following this equation [69]:

$$\frac{e}{a} = \frac{f\,N_i \cdot eN_i + f\,Mn \cdot eMn + f\,Sn \cdot eSn + f\,X \cdot eX}{100} \quad (3)$$

where f Ni, f Mn, f Sn and f X symbolize the atomic fractions of the elements; eNi, eMn, eSn and eX are the corresponding numbers of valence electrons; and X symbolizes the fourth element of a quaternary alloy, respectively.

It is crucial to recognize that for Heusler alloys, (e/a) has a significant influence on the transformation temperatures, considering that the valence electron concentrations per atom are derived through extracting the electron configurations from the outer shells of various elements. Therefore, a linear relationship exists between them, where the e/a ratio is thought to have an impact on the martensite start temperature, M_s. As has been previously established [46], M_s rises with the e/a ratio. Consequently, the two values of M_s and e/a should rise monotonously in accordance with the rule.

For instance, in alloys with the same e/a values, the effects of Ni/Mn ratios on martensitic transformation and magnetic characteristics are comparable [69]. In addition, lowering the e/a value can increase the lattice parameter and cell volume, as stated elsewhere. However, the e/a ratio can be abolished in the case of $Ni_{50-x}Mn_{36}Sn_{14}Pd_x$ alloys due to the substitution of Ni for Pd and the fact that both belong to the same group of the periodic table and the same location of X_2YZ Heusler alloys [1].

The (1 1 0) Brillouin zone is just about to be reached by the Fermi surface, which stabilizes the $L2_1$- austenite structure. Thus, the Fermi surface and the (1 1 0) Brillouin zone will overlap by the increasing of the e/a ratio, and electrons above the Fermi level will then migrate to the corner states of the Brillouin zone. Hereafter, an excessive rise in system energy will influence the formation of martensite by distorting the lattice to diminish the free energy [72]. Because of their linear relationship and prior findings in the literature [73], the martensite start temperature, Ms, is thought to be influenced by the e/a ratio. As a result, the Ms value must follow the rule and increases monotonically with the increase of the e/a ratio, and vice versa. Furthermore, martensitic transformations in $Ni_{50-x}Mn_{37+x}X_{13}$ alloys are found above a critical value of a valence electron concentration of 7.86 [70]. Figure 11 illustrates the linear dependence of Ms as a function of the e/a ratio for several common X_2MnZ Heusler compounds, where the possibility of producing alloys with the thermal hysteresis intervals at the desired temperature range is evidenced by the linear tendency. Moreover, it has been discovered by Jing et al. [74] that in Ni-Mn-Sn-Co Heusler alloys, partial substitution of Ni for Co pushes the martensitic transition to lower temperatures. As stated by Cong et al. [75], when replacing cobalt by nickel in $Ni_{50-x}Co_xMn_{39}Sn_{11}$ alloys, the martensitic transformation temperatures first drops slowly when x= 0, 1, 2, 3 and 4, and then drops quickly when x exceeds 4. They did not detect martensitic transformation in alloys when x exceeded 9. In addition, Coll et al. [76] studied the thermal analysis of $Mn_{50}Ni_{50-x}Sn_x$ (x = 6, 8, and 10) and $Mn_{50}Ni_{50-x}In_x$ (x = 6 and 8) alloys produced by melt spinning. They described that, with an increase in Sn or In content, the transformation changed to lower temperatures. By increasing the Sn and In content, the enthalpy change stabilized its value, whereas the entropy change value increased continuously. Then, the martensitic transition temperature in $Ni_{46.8}Cu_{2.5}Mn_{36.5}Sn_{14.3}$ was detected at around 200 K as the first-order magnetic transition [77]. Commonly, one must refer to the DSC results in order to analyse the thermal stability and to be able to follow the phase transitions carried out in Heusler shape memory alloys; however, one must refer firstly to the XRD results.

As reported above, thermal hysteresis is a typical characteristic for the martensitic transition because of the first-order nature of the transition. Henceforth, in order to notice

the martensite–austenite transition, thermal analysis (DSC scans) must be performed by heating/cooling between room temperature and a temperature higher than the austenite start temperature for alloys that present an austenite phase at room temperature (in XRD spectrums), whereas a cooling/heating rate from room temperature to a temperature lower than the martensitic start temperature for alloys presenting a martensitic phase must be performed [46].

Additional noteworthy features can be extracted from the calorimetric measurements for specific thermodynamic parameters. These include the width of the hysteresis, ΔT, which is characterized by the difference between the peak position's temperatures. Likewise, from the calorimetry data, the entropy change can be calculated by means of the following expression:

$$\Delta S = \frac{1}{T}\left(\frac{dQ}{dt}\right)\left(\frac{dT}{dt}\right)^{-1} dT \quad (4)$$

where the integrals are mathematically calculated from martensitic start temperature on cooling and from austenite finish temperature on heating to a given temperature T in the transformation interval after picking a suitable baseline [46].

By the transformational process, Q is determined to be the heat exchange. It is considered as the DSC peak area and can be equally recognized as the enthalpy change (ΔH) at the temperature that signifies the martensitic transformation (T_0), and the Gibbs energies of martensitic phase are equivalent to the parent phase.

Thus, respecting the thermodynamic equilibrium conditions, the martensitic transformation (T_0) is given by the following expression:

$$T_0 = \frac{1}{2}(Ms + Af) \quad (5)$$

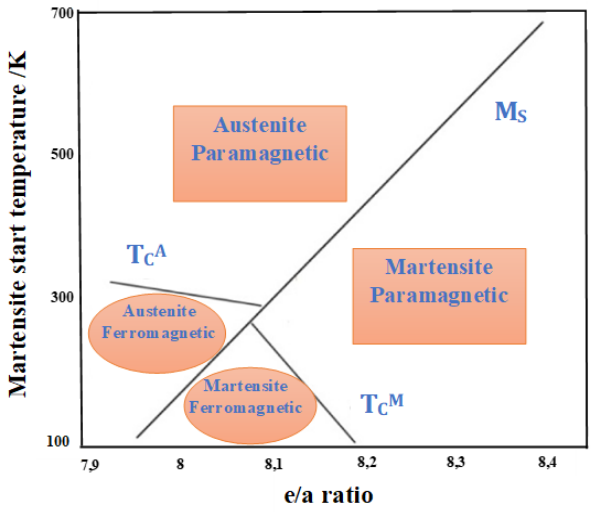

Figure 11. Correlation between the e/a ratio and the martensitic start temperature (Ms).

3.3. Magnetic and Shape Memory Alloys

Moreover, it is conceivable to design an alloy with the adequate temperature range by selecting chemical (and e/a) parameters. However, the e/a ratio is not the only factor that can affect the functional qualities. There are other parameters linked to the functional response, such as magnetic interactions between atoms, the concurrence of the structural and Curie ferromagnetic transformation and so on.

The magnetic properties of Ni-Mn based Heusler alloys can be tuned by varying their composition and crystal structure. The Curie temperature (Tc), which is the temperature above which a material loses its ferromagnetic properties, can be adjusted by tuning the

ratio of Ni and Mn in the alloy, as well as by adding extra elements. Due to the reversibility of the structural transition, a shape memory effect is observed [46]. Moreover, Ni-Mn-based Heusler alloys can also exhibit magneto-striction, which is the change in dimensions of a material when subjected to a magnetic field. This property can be utilized in various applications such as sensors and actuators [46]. For that, Ni-Mn-based Heusler alloys hold great potential for use in various magnetic applications due to their unique magnetic properties that can be tuned by composition and crystal structure. Therefore, in order to determine the transition temperatures and the magnetic state of the alloys, thermomagnetic measurements can be conducted using a vibrating sample magnetometer (VSM) by means of zero-field cooling (ZFC), field-cooling (FC) and field-heating (FH) protocols within a temperature range around the phase transition and by the effect of an applied magnetic field. Several authors have discussed the FC and FH curves behaviors, from which much information can be extracted. For instance, Chabri et al. [57] stated that the presence of a distinct thermal hysteresis of roughly 12 K between FH and FC curves suggests that the martensite transition is of first order in nature in $Ni_{45}Mn_{44}Sn_{11}$ melt-spun ribbons. However, the coincidence of these thermo-magnetization curves close to the Curie temperatures of austenite and martensite phases, T_C^A and T_C^M, respectively, indicates that these transitions are of the second order. From these curves, the typical structural and transition temperatures are noticed as Ms = 261.0 K, Mf = 250.4 K, As = 262.2 K, Af = 274.1 K, T_C^M = 172.0 K, and T_C^A = 307.3 K. Also, it has been discovered elsewhere [78] that the magnetic transformation temperature of the austenite phase (Curie temperature T_C^A) is approximately 325 K for $Ni_{50}Mn_{36}Sn_{14}$ alloys. In the regions of 230 K (Ms)-170 K (Mf) and 195 K (As)-255 K (Af), which correspond to martensitic and reverse martensitic transformations, respectively, dramatic changes in magnetization are seen below T_C^A. Furthermore, the zero-field cooling (ZFC) curve has a blocking temperature TB (65K) as an inflection point that indicates the presence of magnetically inhomogeneous states. The field-cooling (FC) and zero-field cooling (ZFC) curves both split at low temperatures. Generally, this behavior is related to the competition between ferromagnetic (FM) and antiferromagnetic (AFM) systems. Afterwards, with further temperature increases, the magnetization intensity can drop, and the HL vanishes.

Furthermore, it has been noted that MT increases progressively in $Ni_{43}Mn_{46}Sn_{11-x}Te_x$ as Te content increases [71]. This might be explained by the increase in the e/a ratio and the reduction of the unit cell volume. Authors have observed that the Mn atoms that substitute for Sn atoms are coupled anti-ferromagnetically to the ferromagnetic manganese sites. On the other hand, $Ni_{50-x}Cu_xMn_{38}Sn_{12}$ + B3% that are produced in ribbon form by the melt spinning technique have had their manufacturing procedure explained in previous works [1,13,46]. In a previous study, boron was added to the Ni-Mn-Sn system in order to diminish Mn evaporation during the elaboration technique. These Heusler alloys displayed an austenite phase at room temperature, where the Cu substitution for Ni in the Ni-Mn-Sn-B system led to the reduction of the martensitic transformation temperature [63]. A negative magnetoresistance was detected in all the produced ribbons near the martensitic transition. The authors supposed that the magnetic field-induced structural transition could have been responsible for the large magnetoresistance near the martensitic transition. The results attained for the $Ni_{49}Cu_1Mn_{38}Sn_{12}$ + B ribbon showed that the resistances measured at different temperatures dropped suddenly with the rise of the applied magnetic field and overlapped near 80 kOe, thus making the Cu-substituted Mn-Ni-Sn-B based alloys promising candidates for magneto-resistive devices such as magnetic field sensors [63].

By dividing the spin density of Ni into two antiparallel sections, Z integrally displays a relatively poor interaction with its nearby Mn atoms for the $L2_1$ of the alloys with Z = Ni and Cu. Additionally, the Z can create a strong FM coupling with Mn/Mn′ and serve as a mediator between Mn and Mn′ in alloys with an $L2_1$ structure where Z = Co and Fe, which can considerably increase the stability of the FM state. The parallel spin order between the Mn and Mn′, which results from the strong AFM coupling between the Z and Mn/Mn′,

increases the stability of the FM state in the $L2_1$ with Z = Mn and Cr. Similarly, further authors have estimated that the magnetic transition from ferromagnetic (FM) to paramagnetic (PM) state can occur simultaneously with the structural transformation from austenite (AS) to martensite (MS) [79]. Referring to Sun et al. [78], in the $Ni_{50}Mn_{36}Sn_{14}$ Heusler alloy, the temperature at which magnetic transformation occurred was roughly 325 K. In the ranges of 230 K (Ms)–170 K (Mf) and 195 K (As)–255 K (Af), respectively, dramatic changes in magnetization were seen below Curie temperature, which was related to MT and reverse MT. As a further feature, the zero-field cooling (ZFC) curve demonstrated a blocking temperature TB (65 K) inflection point that indicated the presence of magnetically inhomogeneous states. However, the ZFC and FC curves reversibility in $Ni_{2-x}Mn_{1+x}Sb$ demonstrates that the samples are stabilized in a magnetically homogeneous state [80].

The magnetic properties of ferromagnetic Ni-Mn-Sn-Cu ribbons' forms are described elsewhere [46]. The authors concluded that the magneto-structural transition was tuned by an appropriate Cu doping in the alloys. Thus, due to an obvious hysteresis, both FC and ZFC curves exhibited an irreversible behavior, resulting in forward and inverse MT. They stated that the martensitic phase became more stable by increasing an applied magnetic field. Thus, martensite requires more energy from austenite. Related to the ferromagnetic state of the martensite alloy, this makes the MT shift to a higher temperature. The observed ≈3% deformation was entirely restored to the original shape of the material in the $Ni_{45}Co_5Mn_{3.67}In_{13.3}$ compound; this was attributed to a reverse transformation from the antiferromagnetic (or paramagnetic) martensite state to the ferromagnetic parent phase [33]. Because of their very high magnetic field-induced strain (up to 10%) and full shape recovery within $\leq 10^8$ mechanical cycles, Ni–Mn–Ga-based materials are highly suitable for technological applications of magnetic shape memory materials, such as actuators with a long stroke and high precision [81]. The magnetic shape memory alloys lead to a number of important functional properties such as giant magnetoresistance, shape recovery, metamagnetic properties and large magnetocaloric effect.

3.4. Magnetocaloric Effect in Heusler Alloys

Generally, "caloric effect" refers to the application of an external stimulus in a solid material. These stimuli can be applied through a magnetic field (H), hydrostatic pressure (P), mechanical stress (σ) or an electric potential (E), resulting in magnetocaloric, mechanocaloric (barocaloric and elastocaloric) or electrocaloric effects, respectively.

Thus, the magnetocaloric effect (MCE) is the most studied among all caloric effects [82]. The magnetocaloric effect in magnetic refrigeration needs to function around room temperature; hence, the Ms of the Heusler alloys that are susceptible to this effect should be near it [29]. As reported by Pasquale et al. [83], Ni-Mn-Ga alloys have been expansively studied owing to the highest magnetocaloric effect value (ΔS = 86 J/kg /K at 50 KOe field).

In Heusler alloys, the magnetocaloric effect is linked to the magnetic shape memory, which is the reversible martensitic transformation induced by a magnetic field. Buchelnikov et al. [84] stated that the non-stoichiometric $Ni_{2.18}Mn_{0.82}Ga$ and $Ni_{2.19}Mn_{0.81}Ga$ alloys exhibit a highest MC in the vicinity of the ferromagnetic martensite to paramagnetic austenite magneto-structural transition. In addition, in the alloys containing a significant excess of nickel, the change in magnetic entropy turns out to be much smaller. Subsequent studies on almost-stoichiometric Ni–Mn–Ga alloys revealed that the MCE type changed from inverse (entropy change $\Delta S > 0$) to direct (entropy change $\Delta S < 0$) with increasing magnetic field to H > 1 T [85]. As previously mentioned, the presence of the AFM interaction in the Ni–Mn–X (X = In, Sn, and Sb) alloys causes magnetization jumps to appear, which are noticeable in the region of the magnetic structural transition, and effects such as an inverse MCE, giant magnetoresistance and exchange bias effect are observed [82].

Likewise, the inverse magnetocaloric effect can be perceived in some Heusler alloys. This is the most typical case. In this instance, a rise in the magnetic field allows the decrease of the temperature. Therefore, Krenke et al. [86] established the initial observation

of the inverse magnetocaloric effect in $Ni_{0.50}Mn_{0.50-x}Sn_x$ alloys. It was demonstrated that the structural and magnetic phase transformation took place in the range of composition of $0.13 \leq x \leq 0.15$. Additionally, they examined the field-induced entropy change (ΔS) at various compositions around the martensitic transition. The compositions with x = 0.15 and × = 0.13 revealed a positive entropy change between $Mf \leq T \leq Ms$. Therefore, the entropy variation as a function of temperature for the highest applied magnetic field (5 T) was 15 J/ K/kg for x = 0.15 and 18 J /K/kg for x = 0.13. Furthermore, other Heusler alloys exhibit the inverse magnetocaloric effect such as Ni-Mn-In-X [87] and Ni-Mn-Sn-X [88].

3.5. Additional Properties and Applications of Heusler Alloys

Heusler materials are commonly categorized into three distinct groups based on their electronic properties: metals, known for their ability to conduct electricity; topological insulators; and semiconductors or semimetals [89]. Given that they combine metallic behavior at the surface and insulating behavior in the bulk, topological insulators are classified as part of a novel class of materials that cannot be solely categorized as insulators, semiconductors or metals, offering promise for innovative spintronic and quantum computing applications [90].

These distinctions arise from the features of their valence and conduction bands. In materials where the valence band is fully occupied and separated from the conduction band by an energy gap, the material can act as either an insulator or a semiconductor. Insulating materials present a significant energy gap between their valence and conduction bands, preventing electrons excitation between them [90]. Conversely, they possess a smaller band gap compared to insulators, allowing for the migration of electrons from the valence to the conduction band under suitable conditions. In the case of metals, there is an overlap between the valence and conduction bands, leading to no defined band gap. This overlapping enables electron conductivity from absolute zero temperature (0 K) up to finite temperatures [32].

The electronic structures of full and half Heusler compounds are relatively different. In order for full Heusler to achieve semiconductor status, a total of 24 valence electrons are required for the electron in the outermost layer to reach a full shell state, like Fe_2VAl. Ferromagnetism, ferrimagnetism or antiferromagnetism will manifest when the total number of valence electrons is not 24 [29].

Once the total number of valence electrons in the half-Heusler compound is 18, it will act as a semiconductor [89]. However, compounds in which the total number of valence electrons is less than 18 tend to transform into metals or magnetic materials.

The majority of them, including FeMnSb, CrMnSb, and MnCoSb, do not yet crystallize in the C1b configuration; that instability results from the electrons of Mn ions being partially bonded within the ions and owing to the fact that they include multiple magnetic elements. Several semi metallic ferromagnets, such NiMnSb and PtMnSb, are an exception to the rule and will crystallize in the C1b configuration. These semimetals can display both metal and insulator qualities in the same material, depending on the distinct spin directions [91].

Considering thermoelectric characteristics, half-Heusler compounds exhibit more obvious thermoelectric characteristics than FH, including a greater Curie temperature and spin polarizability. Additionally, as indirect bandgap semiconductors having bandgaps of 0.91 eV and 0.82 eV, respectively, the half-Heusler PdZrSn and PdHfSn materials and PdHfSn have demonstrated a strong thermoelectric performance [92]. Since thermoelectric materials permit direct energy conversion between heat and electricity and vice versa, they could be promising approaches for solid-state cooling and waste heat recovery applications [93].

Moreover, Heusler compound's thermoelectric effectiveness can be enhanced by doping it or by adding a giant anomalous Nernst transverse thermoelectric effect. In addition, the Heusler compounds may develop into topological superconductors [94]. In this context, unexpectedly, half-Heusler semimetals of YPtBi and LuPtBi have already been

proven to exhibit topological superconductivity by Lui et al. [95]. The non-centrosymmetric crystal structure resulting from symmetry breaking and band inversion is the root cause of the topological surface states of LuPtBi and YPtBi [96].

Certain alloys exhibit superconductivity at low temperatures, showcasing potential applications in high-performance electronics and energy storage. Among them, the YPtBi surface state exhibits superconductivity below the critical temperature Tc = 0.77 K, and at Hc(0) = 1.5 T, the positive charge carrier density is incredibly low [97]. However, the LuPtBi surface state's superconductivity occurs below Tc = 1.0 K and Hc(0) = 1.6 T [96]. According to several studies, the element composition of XPtBi (a rare earth element) tends to become a semiconductor when X is a light rare earth element, a semimetal when X is heavy and only a semimetal when the orbital spin coupling interaction occurs [91]. Moreover, there exists topological superconductivity in HoPdBi, LnPd2Sn (Ln = Sc, Y, Lu) and other full- and half-Heusler materials [98].

Overall, the topological insulators hold significant potential for revolutionizing various technological fields, from electronics to quantum computing, owing to their exotic electronic properties and robust surface states.

Concerning the applications areas, spintronics, also known as spin electronics, is a new discipline of solid-state physics devoted to investigating the impact of spin currents on electrical conduction, which was discovered during the last three decades [99]. Spintronics has proven to offer several advantages over conventional electrical devices, including higher integration densities, rise in data processing rates, universal memory and lower electric power consumption [100]. The development of devices with a greatest tunneling magnetoresistance effect is the key objective of spintronics. A pair of approaches exist for achieving this objective: the first is creating an insulating barrier, while the second involves using novel 100% spin-polarized materials instead of a conventional magnetic electrode [101]. Half-metallic ferromagnetic oxides and half-metallic ferromagnetic metals, such as Heusler compounds, are potential candidates [100].

Co_2YZ Heusler alloys, in particular, have attracted an extensive interest for their use in spintronic applications owing to their high Curie temperature and half metallicity [102–104]. Thin films of these alloys have been extensively explored in magnetic tunnel junctions in arrangement with an MgO barrier. For magnetic tunnel junctions, Inomata et al. [105] created a film by growing the Quaternary Heusler alloy $Co_2FeSi_{1-x}Al_x$ epitaxially on an MgO (0 0 1) substrate. High magnification showed the magnetic tunnel junction's good-quality morphology, and the top and lower Heusler alloy's and MgO barrier's outstanding epitaxial plane matching were observed. The magnetoresistance values at room temperature and 5 K were found to be 200% and 380%, respectively. Furthermore, the XRD results showed that the annealing at temperatures over 450 °C produced the $L2_1$ structure in the film, while annealing at temperatures lower than 400 °C produced the B2 structure. Overall, Heusler alloys offer a wide range of possibilities for various technological applications, as presented in Figure 12, and ongoing research continues to explore and exploit their unique properties for practical use in different fields.

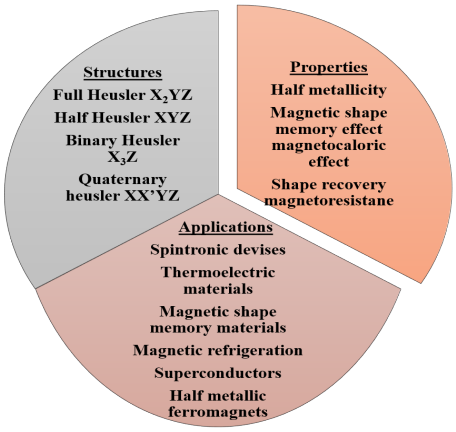

Figure 12. List of different structures, properties and possible applications of Heusler alloys.

4. Conclusions

The overview of this paper is devoted to a review of current research investigations on structural, phase transitions and thermal properties of ternary Ni–Mn–X and quaternary Ni-Mn-Sn-X Heusler compounds. Furthermore, this review underlines the importance of Heusler alloys in diverse applications, ranging from magnetic and spintronic devices to thermoelectric materials. The authors expertly navigate through the complexities of structural changes and phase transitions, offering insights that could facilitate the design and optimization of Heusler alloys for specific functionalities. Several multifunctional properties have been identified in these systems, such as the shape memory effect, extraordinary magnetocaloric effect, large magnetoresistance, the superparamagnetic effect and associated ferromagnetic-antiferromagnetic characteristics. We contend that future studies ought to focus on the atomic site occupancy and atomic order rules of these types of alloys and specifically off-stochiometric ones. Also, further studies remain to be conducted concerning the effects of various synthesis procedures and thermal annealing techniques on the development of the ordered $L2_1$ phase.

Author Contributions: Substantial contributions to the Conception of the work, L.E. and J.S.; methodology, A.W. and L.E.; validation, J.-J.S. and J.S.; writing—original draft preparation, A.W. and W.B.M.; formal analysis, A.W. and W.B.M.; Investigation, A.W. and J.D.; review and editing, J.D. and J.-J.S. supervision, L.E. J.S. and J.-J.S. All authors have read and agreed to the published version of the manuscript. All authors have agreed to be accountable for all aspects of the work in ensuring that questions related to the accuracy or integrity of any part of the work are appropriately investigated and resolved.

Funding: This research received no external funding.

Data Availability Statement: It is a review; data are available by requesting the authors.

Acknowledgments: A. Wederni agrees a UdG postdoctoral contact and J. Daza a Agaur Joan Oró grant.

Conflicts of Interest: The authors declare no conflicts of interest.

References

1. Wederni, A.; Ipatov, M.; Pineda, E.; Escoda, L.; González, J.-M.; Khitouni, M.; Suñol, J.-J. Martensitic Transformation, Thermal Analysis and Magnetocaloric Properties of Ni-Mn-Sn-Pd Alloys. *Processes***2020**, *8*, 1582, doi:10.3390/pr8121582.
2. Mohd Jani, J.; Leary, M.; Subic, A.; Gibson, M.A. A Review of Shape Memory Alloy Research, Applications and Opportunities. *Mater. Des.***2014**, *56*, 1078–1113, doi:10.1016/j.matdes.2013.11.084.
3. Zhang, K.; Tan, C.; Guo, E.; Feng, Z.; Zhu, J.; Tong, Y.; Cai, W. Simultaneous Tuning of Martensitic Transformation Behavior, Magnetic and Mechanical Properties in Ni–Mn–Sn Magnetic Alloy by Cu Doping. *J Mater Chem C Mater***2018**, *6*, 5228–5238, doi:10.1039/C7TC05440H.

4. Lu, H.Z.; Liu, L.H.; Yang, C.; Luo, X.; Song, C.H.; Wang, Z.; Wang, J.; Su, Y.D.; Ding, Y.F.; Zhang, L.C.; et al. Simultaneous Enhancement of Mechanical and Shape Memory Properties by Heat-Treatment Homogenization of Ti2Ni Precipitates in TiNi Shape Memory Alloy Fabricated by Selective Laser Melting. *J Mater Sci Technol***2022**, *101*, 205–216, doi:10.1016/J.JMST.2021.06.019.
5. Trehern, W.; Ortiz-Ayala, R.; Atli, K.C.; Arroyave, R.; Karaman, I. Data-Driven Shape Memory Alloy Discovery Using Artificial Intelligence Materials Selection (AIMS) Framework. *Acta Mater***2022**, *228*, 117751, doi:10.1016/J.ACTAMAT.2022.117751.
6. Gusarov, B.; Gusarova, E.; Viala, B.; Gimeno, L.; Boisseau, S.; Cugat, O.; Vandelle, E.; Louison, B. Thermal Energy Harvesting by Piezoelectric PVDF Polymer Coupled with Shape Memory Alloy. *Sens Actuators A Phys* **2016**, *243*, 175–181, doi:10.1016/J.SNA.2016.03.026.
7. Huang, X.M.; Wang, L. Da; Liu, H.X.; Yan, H. Le; Jia, N.; Yang, B.; Li, Z. Bin; Zhang, Y.D.; Esling, C.; Zhao, X.; et al. Correlation between Microstructure and Martensitic Transformation, Mechanical Properties and Elastocaloric Effect in Ni–Mn-Based Alloys. *Intermetallics (Barking)* **2019**, *113*, 106579, doi:10.1016/j.intermet.2019.106579.
8. Bachagha, T.; Daly, R.; Khitouni, M.; Escoda, L.; Saurina, J.; Suñol, J. Thermal and Structural Analysis of Mn49.3Ni43.7Sn7.0 Heusler Alloy Ribbons. *Entropy* **2015**, *17*, 646–657, doi:10.3390/e17020646.
9. Wen, J.; Yang, B.; Dong, Z.; Yan, Y.; Zhao, X. Manipulation of the Martensitic Transformation and Exchange Bias Effect in the Ni45Co5Mn37In13 Ferromagnetic Shape Memory Alloy Films. *Magnetochemistry 2023, Vol. 9, Page 51* **2023**, *9*, 51, doi:10.3390/MAGNETOCHEMISTRY9020051.
10. Goswami, D.; Chattopadhyay, S.; Das, J. Effect of the Post Annealing Cooling Rate on the Martensitic Transformation and the Magnetocaloric Effect in Ni-Mn-Sn Ribbons. *Mater Res Bull* **2023**, *160*, 112129, doi:10.1016/J.MATERRESBULL.2022.112129.
11. Dadda, K.; Alleg, S.; Souilah, S.; Suňol, J.J.; Dhahri, E.; Bessais, L.; Hlil, E.K. Critical Behavior, Magnetic and Magnetocaloric Properties of Melt-Spun Ni50Mn35Sn15ribbons. *J Alloys Compd* **2018**, *735*, 1662–1672, doi:10.1016/j.jallcom.2017.11.277.
12. Modak, R.; Raja, M.M.; Srinivasan, A. Enhanced Magneto-Caloric Effect upon Fourth Element (Cu, Fe, Co) Substitution in Ni–Mn–Sn Thin Films. *Applied Physics A* **2019**, *125*, 57, doi:10.1007/s00339-018-2340-8.
13. Wederni, A.; Ipatov, M.; González, J.M.; Khitouni, M.; Suñol, J.J. Ni-Mn-Sn-Cu Alloys after Thermal Cycling: Thermal and Magnetic Response. *Materials***2021**, *14*, doi:10.3390/MA14226851.
14. Graf, T.; Casper, F.; Winterlik, J.; Balke, B.; Fecher, G.H.; Felser, C. Crystal Structure of New Heusler Compounds. *Z Anorg Allg Chem* **2009**, *635*, 976–981, doi:10.1002/ZAAC.200900036.
15. Heusler, O. Kristallstruktur Und Ferromagnetismus Der Mangan-Aluminium-Kupferlegierungen. *Ann Phys* **1934**, *411*, 155–201, doi:10.1002/ANDP.19344110205.
16. Salaheldeen, M.; Wederni, A.; Ipatov, M.; Gonzalez, J.; Zhukova, V.; Zhukov, A. Elucidation of the Strong Effect of the Annealing and the Magnetic Field on the Magnetic Properties of Ni2-Based Heusler Microwires. *Crystals (Basel)* **2022**, *12*, doi:10.3390/CRYST12121755.
17. Salaheldeen, M.; Garcia-Gomez, A.; Ipatov, M.; Corte-Leon, P.; Zhukova, V.; Blanco, J.M.; Zhukov, A. Fabrication and Magneto-Structural Properties of Co2-Based Heusler Alloy Glass-Coated Microwires with High Curie Temperature. *Chemosensors 2022, Vol. 10, Page 225***2022**, *10*, 225, doi:10.3390/CHEMOSENSORS10060225.
18. Datta, S.; Kar, M. NiMnSn Half Heusler Alloy: Critical Phenomena at the Ferromagnetic to Paramagnetic Phase Transition. *Mater Today Proc***2022**, *57*, 431–435, doi:10.1016/J.MATPR.2021.12.540.
19. Chen, C.; Yu, L.; Zhu, J.; Tan, C. The Mechanical Properties of Ni-Mn-Sn Alloy Thin Films with Fe Doping. *Integrated Ferroelectrics* **2020**, *207*, 156–165, doi:10.1080/10584587.2020.1728675.
20. Gruner, M.E.; Niemann, R.; Entel, P.; Pentcheva, R.; Rößler, U.K.; Nielsch, K.; Fähler, S. Modulations in Martensitic Heusler Alloys Originate from Nanotwin Ordering. *Sci Rep* **2018**, *8*, doi:10.1038/s41598-018-26652-6.
21. Resnina, N.; Belyaev, S.; Shelyakov, A.; Ubyivovk, E. Violation of the Sequence of Martensite Crystals Formation on Cooling and Their Shrinking on Heating during B2 ↔ B19′ Martensitic Transformation in Ti40.7Hf9.5Ni44.8Cu5 Shape-Memory Alloy. *Phase Transitions* **2017**, *90*, 289–298, doi:10.1080/01411594.2016.1180517.
22. Bachagha, T.; Suñol, J.J. All-d-Metal Heusler Alloys: A Review. *Metals 2023, Vol. 13, Page 111* **2023**, *13*, 111, doi:10.3390/MET13010111.
23. Wei, Z.Y.; Liu, E.K.; Chen, J.H.; Li, Y.; Liu, G.D.; Luo, H.Z.; Xi, X.K.; Zhang, H.W.; Wang, W.H.; Wu, G.H. Realization of Multifunctional Shape-Memory Ferromagnets in All- d -Metal Heusler Phases. *Appl Phys Lett* **2015**, *107*, 22406, doi:10.1063/1.4927058/29544.
24. Roy, S.; Blackburn, E.; Valvidares, S.M.; Fitzsimmons, M.R.; Vogel, S.C.; Khan, M.; Dubenko, I.; Stadler, S.; Ali, N.; Sinha, S.K.; et al. Delocalization and Hybridization Enhance the Magnetocaloric Effect in Cu-Doped Ni2 MnGa. *Phys Rev B Condens Matter Mater Phys* **2009**, *79*, 235127, doi:10.1103/PHYSREVB.79.235127/FIGURES/4/MEDIUM.
25. Wederni, A.; Salaheldeen, M.; Ipatov, M.; Zhukova, V.; Zhukov, A. Influence of the Geometrical Aspect Ratio on the Magneto-Structural Properties of Co2MnSi Microwires. *Metals* **2023**, *13*, 1692, doi:10.3390/MET13101692.
26. Salaheldeen, M.; Wederni, A.; Ipatov, M.; Zhukova, V.; Zhukov, A. Preparation and Magneto-Structural Investigation of High-Ordered (L21 Structure) Co2MnGe Microwires. *Processes 2023, Vol. 11, Page 1138* **2023**, *11*, 1138, doi:10.3390/PR11041138.
27. Meyers, M.A.; Ruud, C.O.; Barrett, C.S. Observations on the Ferromagnetic β Phase of the Cu–Mn–Sn System. *J Appl Crystallogr* **1973**, *6*, 39–41, doi:10.1107/S0021889873008022.
28. Graf, T.; Parkin, S.S.P.; Felser, C. Heusler Compounds - A Material Class with Exceptional Properties. *IEEE Trans Magn* **2011**, *47*, 367–373, doi:10.1109/TMAG.2010.2096229.

29. Tavares, S.; Yang, K.; Meyers, M.A. Heusler Alloys: Past, Properties, New Alloys, and Prospects. *Prog Mater Sci* **2023**, *132*, 101017, doi:10.1016/J.PMATSCI.2022.101017.
30. He, X.; Kang, Y.; Wei, S.; Zhang, Y.; Cao, Y.; Xu, K.; Li, Z.; Jing, C.; Li, Z. A Large Barocaloric Effect and Its Reversible Behavior with an Enhanced Relative Volume Change for Ni42.3Co7.9Mn38.8Sn11 Heusler Alloy. *J Alloys Compd* **2018**, *741*, 821–825, doi:10.1016/J.JALLCOM.2018.01.244.
31. Elphick, K.; Frost, W.; Samiepour, M.; Kubota, T.; Takanashi, K.; Sukegawa, H.; Mitani, S.; Hirohata, A. Heusler Alloys for Spintronic Devices: Review on Recent Development and Future Perspectives. *Sci Technol Adv Mater* **2021**, *22*, 235–271, doi:10.1080/14686996.2020.1812364.
32. Khandy, S.A.; Islam, I.; Wani, A.F.; Ali, A.M.; Sayed, M.A.; Srinavasan, M.; Kaur, K. Strain Dependent Electronic Structure, Phonon and Thermoelectric Properties of CuLiX (X=S,Te) Half Heusler Compounds. *Physica B Condens Matter* **2024**, *677*, 415698, doi:10.1016/J.PHYSB.2024.415698.
33. Graf, T.; Felser, C.; Parkin, S.S.P. Simple Rules for the Understanding of Heusler Compounds. *Progress in Solid State Chemistry* **2011**, *39*, 1–50, doi:10.1016/J.PROGSOLIDSTCHEM.2011.02.001.
34. Wjin, H.P.J. Alloys and Compounds of d-Elements with Main Group Elements. Part 2, Springer, **1988**, doi:10.1007/B33550.
35. Životský, O.; Skotnicová, K.; Čegan, T.; Juřica, J.; Gembalová, L.; Zažímal, F.; Szurman, I. Structural and Magnetic Properties of Inverse-Heusler Mn2FeSi Alloy Powder Prepared by Ball Milling. *Materials 2022, Vol. 15, Page 697* **2022**, *15*, 697, doi:10.3390/MA15030697.
36. Zhang, Q.; Huang, G.; Li, S. Mechanical Properties of DO3 Based on First Principles. *Crystals* **2020**, *10*, 488, doi:10.3390/CRYST10060488.
37. Liu, H.; Gao, G.Y.; Hu, L.; Ni, Y.; Zu, F.; Zhu, S.; Wang, S.; Yao, K.L. Bulk and Surface Half-Metallicity: The Case of D03-Type Mn3Ge. *J Appl Phys* **2014**, *115*, 33704, doi:10.1063/1.4861875/829325.
38. Hebri, S.; Abdelli, A.-B.; Belfedal, N.; Bensaid, D. Investigating the Structural, Electronic, and Elastic Properties of Li-Based Quaternary Heusler Alloy Semiconductors Using Hybrid Functional-HSE06 Bandgap Recalculations. *Inorg Chem Commun***2023**, *150*, 110479, doi:10.1016/j.inoche.2023.110479.
39. Galanakis, I.; H. Dederichs, P. Half-Metallicity and Slater-Pauling Behavior in the Ferromagnetic Heusler Alloys in Half-Metallic alloys, Springer,. **2006**, 1–39, doi:10.1007/11506256_1.
40. Salaheldeen, M.; Wederni, A.; Ipatov, M.; Zhukova, V.; Anton, R.L.; Zhukov, A. Enhancing the Squareness and Bi-Phase Magnetic Switching of Co2FeSi Microwires for Sensing Application. *Sensors 2023, Vol. 23, Page 5109,* **2023**, doi:10.3390/S23115109.
41. Balke, B.; Wurmehl, S.; Fecher, G.H.; Felser, C.; Kübler, J. Rational Design of New Materials for Spintronics: Co2FeZ (Z=Al, Ga, Si, Ge). *Sci Technol Adv Mater* **2008**, *9*, doi:10.1088/1468-6996/9/1/014102.
42. Kumar, A.; Pan, F.; Husain, S.; Akansel, S.; Brucas, R.; Bergqvist, L.; Chaudhary, S.; Svedlindh, P. Temperature-Dependent Gilbert Damping of Co2FeAl Thin Films with Different Degree of Atomic Order. *Phys Rev B***2017**, *96*, 224425, doi:10.1103/PHYSREVB.96.224425/FIGURES/8/MEDIUM.
43. Özduran, M.; Candan, A.; Akbudak, S.; Kushwaha, A.K.; İyigör, A. Structural, Elastic, Electronic, and Magnetic Properties of Si-Doped Co2MnGe Full-Heusler Type Compounds. *J Alloys Compd* **2020**, *845*, 155499, doi:10.1016/J.JALLCOM.2020.155499.
44. Koch, D.; Beckmann, B.; Fortunato, N.M.; Miroshkina, O.N.; Gruner, M.E.; Zhang, H.; Gutfleisch, O.; Donner, W. Chemical Long Range Ordering in All-d-Metal Heusler Alloys. *J Appl Phys* **2022**, *131*, 73903, doi:10.1063/5.0079952/2836398.
45. Wei, Z.Y.; Liu, E.K.; Li, Y.; Han, X.L.; Du, Z.W.; Luo, H.Z.; Liu, G.D.; Xi, X.K.; Zhang, H.W.; Wang, W.H.; et al. Magnetostructural Martensitic Transformations with Large Volume Changes and Magneto-Strains in All- d -Metal Heusler Alloys. *Appl Phys Lett* **2016**, *109*, 71904, doi:10.1063/1.4961382/32515.
46. Wederni, A.; Ipatov, M.; Pineda, E.; Suñol, J.-J.; Escoda, L.; González, J.M.; Alleg, S.; Khitouni, M.; Żuberek, R.; Chumak, O.; et al. Magnetic Properties, Martensitic and Magnetostructural Transformations of Ferromagnetic Ni–Mn–Sn–Cu Shape Memory Alloys. *Applied Physics A***2020**, *126*, 320, doi:10.1007/s00339-020-03489-3.
47. Qiu, P.; Yang, J.; Huang, X.; Chen, X.; Chen, L. Effect of Antisite Defects on Band Structure and Thermoelectric Performance of ZrNiSn Half-Heusler Alloys. *Appl Phys Lett* **2010**, *96*, 152105, doi:10.1063/1.3396981/338879.
48. Jodin, L.; Tobola, J.; Pecheur, P.; Scherrer, H.; Kaprzyk, S. Effect of Substitutions and Defects in Half-Heusler FeVSb Studied by Electron Transport Measurements and KKR-CPA Electronic Structure Calculations., doi:10.1103/PhysRevB.70.184207.
49. Kumar, A.; Chaudhary, S.; Chandra, S. Effect of Point Defects and Lattice Distortions on the Structural, Electronic, and Magnetic Properties of Co2MnAl Heusler Alloy. *Physical Review Materials* **2024**, *8*, 034405.
50. Zhang, H.; Liu, W.; Lin, T.; Wang, W.; Liu, G. Phase Stability and Magnetic Properties of Mn3Z (Z = Al, Ga, In, Tl, Ge, Sn, Pb) Heusler Alloys. *Applied Sciences* **2019**, *9*, 964, doi:10.3390/APP9050964.
51. Chen, P.; Yan, Z.; Liu, X.; Cao, D.; Gao, D.; Gao, C. Tetragonal Distortion Modified Magnetism and Anomalous Hall Effect of Mn 2 CoAl Heusler Alloys through Ar Ion Irradiation. *Journal of Physics D: Applied Physics J. Phys. D: Appl. Phys* **2022**, *55*, 6, doi:10.1088/1361-6463/ac9149.
52. Rekik, H.; Krifa, M.; Bachaga, T.; Escoda, L.; Sunol, J.J.; Khitouni, M.; Chmingui, M. Structural and Martensitic Transformation of MnNiSn Shape Memory Alloys. *International Journal of Advanced Manufacturing Technology* **2017**, *90*, doi:10.1007/s00170-016-9365-y.
53. Chatterjee, S.; Giri, S.; De, S.K.; Majumdar, S. Reentrant-Spin-Glass State in Ni2Mn1.36Sn0.64 Shape-Memory Alloy .*Phys Rev B* **2009**, *79*, doi:10.1103/physrevb.79.092410.

54. Louidi, S.; Suñol, J.J.; Bachagha, T.; González-Legarreta, L.; Rosa, W.O.; Hernando, B. Thermomagnetic and Structural Analysis of As-Quenched Ni49Co1Mn37Sn13. *Physica Status Solidi (C) Current Topics in Solid State Physics***2014**, *11*, 1116–1119, doi:10.1002/pssc.201300700.
55. Zhang, K.; Tian, X.; Tan, C.; Guo, E.; Zhao, W.; Cai, W. Designing a New Ni-Mn-Sn Ferromagnetic Shape Memory Alloy with Excellent Performance by Cu Addition. *Metals* **2018**, *8*, 152, doi:10.3390/MET8030152.
56. Hernando, B.; Llamazares, J.L.S.; Santos, J.D.; Sánchez, M.L.; Escoda, Ll.; Suñol, J.J.; Varga, R.; García, C.; González, J. Grain Oriented NiMnSn and NiMnIn Heusler Alloys Ribbons Produced by Melt Spinning: Martensitic Transformation and Magnetic Properties. *J Magn Magn Mater***2 009**, *321*, 763–768, doi:10.1016/j.jmmm.2008.11.105.
57. Chabri, T.; Venimadhav, A.; Nath, T.K. Magnetic and Lattice Entropy Change across Martensite Transition of Ni-Mn-Sn Melt Spun Ribbons: Key Factors in Magnetic Refrigeration. *J Magn Magn Mater* **2018**, *466*, 385–392, doi:10.1016/J.JMMM.2018.07.048.
58. Chabri, T.; Venimadhav, A.; Nath, T.K. Interplay of Austenite and Martensite Phase inside Martensite Transition Regime and Its Role on Magnetocaloric Effect and Magnetoresistance in Ni-Mn-Sn Based Heusler Alloy. *Intermetallics (Barking)* **2018**, *102*, 65–71, doi:10.1016/J.INTERMET.2018.09.003.
59. Krenke, T.; Moya, X.; Aksoy, S.; Acet, M.; Entel, P.; Mañosa, Ll.; Planes, A.; Elerman, Y.; Yücel, A.; Wassermann, E.F. Electronic Aspects of the Martensitic Transition in Ni–Mn Based Heusler Alloys. *J Magn Magn Mater* **2007**, *310*, 2788–2789, doi:10.1016/J.JMMM.2006.10.1139.
60. Friák, M.; Zelený, M.; Mazalová, M.; Miháliková, I.; Turek, I.; Kaštil, J.; Kamarád, J.; Míšek, M.; Arnold, Z.; Schneeweiss, O.; et al. The Impact of Disorder on the 4O-Martensite of Ni–Mn–Sn Heusler Alloy. *Intermetallics (Barking)* **2022**, *151*, 107708, doi:10.1016/J.INTERMET.2022.107708.
61. Wang, X.; Shang, J.X.; Wang, F.H.; Jiang, C.B.; Xu, H. Bin Effect of 3d Transition Elements Substitution for Ni in Ni2Mn1+xSn1-x on the Phase Stability and Magnetic Properties: A First Principle Investigation. *J Magn Magn Mater* **2014**, *368*, 286–294, doi:10.1016/J.JMMM.2014.05.040.
62. Jiang, Y.; Li, Z.; Li, Z.; Yang, Y.; Yang, B.; Zhang, Y.; Esling, C.; Zhao, X.; Zuo, L. Magnetostructural Transformation and Magnetocaloric Effect in Mn-Ni-Sn Melt-Spun Ribbons., doi:10.1140/epjp/i2017-11316-1.
63. Kirat, G.; Ali Aksan, M. Investigation of Martensitic Transformation and Magnetoresistance Properties of Cu-Substituted Ni-Mn-Sn-B Melt Spun Ribbons. *J Magn Magn Mater* **2021**, *529*, 167858, doi:10.1016/J.JMMM.2021.167858.
64. Das, R.; Sarma, S.; Perumal, A.; Srinivasan, A. Effect of Co and Cu Substitution on the Magnetic Entropy Change in Ni46Mn43Sn11 Alloy. *J Appl Phys* **2011**, *109*, 07A901, doi:10.1063/1.3540327.
65. Finley, J, Lee C.H., Pinshane, Y., Liu, H.L. Spin-Orbit Torque Switching in a Nearly Compensated Heusler Ferrimagnet., doi:10.1002/adma.201805361.
66. Xu, Y.; Xu, C.; Yang, D.; Zhang, R.; Huang, X.; Jiang, Y.; Yu, G.; Pan, L. Crystalline and Magnetic Structures and Ferromagnetic Resonance Study of Ni-Co-Mn-Ge Heusler Alloy System. **2017**, doi:10.1016/j.jallcom.2017.12.105.
67. Zhang, K.; Tan, C.; Zhao, W.; Guo, E.; Tian, X. Computation-Guided Design of Ni-Mn-Sn Ferromagnetic Shape Memory Alloy with Giant Magnetocaloric Effect and Excellent Mechanical Properties and High Working Temperature via Multielement Doping. *ACS Appl Mater Interfaces* **2019**, *11*, 34827–34840, doi:10.1021/ACSAMI.9B08640/ASSET/IMAGES/LARGE/AM9B08640_0020.JPEG.
68. Svetlana, E. Kulkova.; Sergey, V. Eremeev.; Tomoyuki, Kakeshita.; Sergey, S. Kulkov.; and Gennadiy, E. Rudenski. The Electronic Structure and Magnetic Properties of Full- and Half-Heusler Alloys. *Mat Trans* **2006**, *47*, 599-606, doi.org/10.2320/matertrans.47.599.
69. Khan, R.A.A.; Ghomashchi, R.; Xie, Z.; Chen, L. Ferromagnetic Shape Memory Heusler Materials: Synthesis, Microstructure Characterization and Magnetostructural Properties. *Materials* **2018**, *11*, 988, doi:10.3390/MA11060988.
70. Rama Rao, N. V.; Chandrasekaran, V.; Suresh, K.G. Effect of Ni/Mn Ratio on Phase Transformation and Magnetic Properties in Ni–Mn–In Alloys. *J Appl Phys* **2010**, *108*, 043913, doi:10.1063/1.3467966.
71. Archana, R.; Kavita, S.; Ramakrishna, V. V.; Kumar, V.S.; Bhatt, P.; Yusuf, S.M.; Gopalan, R. Successive, Overlapping Transitions and Magnetocaloric Effect in Te Doped Ni-Mn-Sn Heusler Alloys. *J Alloys Compd* **2023**, *947*, 169434, doi:10.1016/j.jallcom.2023.169434.
72. Zheng, H.; Wang, W.; Xue, S.; Zhai, Q.; Frenzel, J.; Luo, Z. Composition-Dependent Crystal Structure and Martensitic Transformation in Heusler Ni–Mn–Sn Alloys. *Acta Mater* **2013**, *61*, 4648–4656, doi:10.1016/J.ACTAMAT.2013.04.035.
73. Louidi, S.; Suñol, J.J.; Ipatov, M.; Hernando, B. Effect of Cobalt Doping on Martensitic Transformations and the Magnetic Properties of Ni50−xCoxMn37Sn13 (x = 1, 2, 3) Heusler Ribbons. *J Alloys Compd* **2018**, *739*, 305–310, doi:10.1016/J.JALLCOM.2017.12.280.
74. Jing, C.; Li, Z.; Zhang, H.L.; Chen, J.P.; Qiao, Y.F.; Cao, S.X.; Zhang, J.C. Martensitic Transition and Inverse Magnetocaloric Effect in Co Doping Ni–Mn–Sn Heusler Alloy. *The European Physical Journal B* **2009**, *67*, 193–196, doi:10.1140/EPJB/E2009-00023-9.
75. Cong, D.Y.; Roth, S.; Schultz, L. Magnetic Properties and Structural Transformations in Ni-Co-Mn-Sn Multifunctional Alloys. *Acta Mater* **2012**, *60*, 5335–5351, doi:10.1016/j.actamat.2012.06.034.
76. Coll, R.; Saurina, J.; Escoda, L.; Suñol, J.J. Thermal Analysis of Mn50Ni50−x(Sn, In)x Heusler Shape Memory Alloys. *J Therm Anal Calorim* **2018**, *134*, 1277–1284, doi:10.1007/S10973-018-7551-X/TABLES/3.
77. Yüzüak, E. The Magnetothermal Characterization of Ni-Cu-Mn-Sn Alloy. *Mater Res Bull* **2021**, *142*, 111398, doi:10.1016/J.MATERRESBULL.2021.111398.

78. Sun, H.; Jing, C.; Zeng, H.; Su, Y.; Yang, S.; Zhang, Y.; Bachagha, T.; Zhou, T.; Hou, L.; Ren, W. Martensitic Transformation, Magnetic and Mechanical Characteristics in Unidirectional Ni–Mn–Sn Heusler Alloy. *Magnetochemistry 2022, Vol. 8, Page 136***2022**, *8*, 136, doi:10.3390/MAGNETOCHEMISTRY8100136.
79. N, Elwindari; C, Kurniawan; A, Manaf. Phase transition of Ni43Mn41Co5Sn11 Heusler alloy. *AIP Conf. Proc* **2017**, *1862*, 030060, doi.org/10.1063/1.4991164.
80. Govind, B.; Bharti, P.; Srivastava, M.; Kumar, A.; Bano, S.; Bhatt, K.; Tawale, J.S.; Pulikkotil, J.J.; Misra, D.K. Magnetic Properties of Intermediate Ni2-XMn1+xSb Full-Heusler Compounds. *Mater Res Bull* **2021**, *142*, 111427, doi:10.1016/j.materresbull.2021.111427.
81. Chmielus, M.; Chernenko, V.A.; Knowlton, W.B.; Kostorz, G.; Müllner, P. Training, Constraints, and High-Cycle Magneto-Mechanical Properties of Ni-Mn-Ga Magnetic Shape-Memory Alloys. *European Physical Journal: Special Topics***2008**, *158*, 79–85, doi:10.1140/epjst/e2008-00657-3.
82. Planes, A.; Mañosa, L.; Acet, M. Magnetocaloric Effect and Its Relation to Shape-Memory Properties in Ferromagnetic Heusler. *Journal of Physics: Condensed Matter* **2009**, *21*, 233201, doi:10.1088/0953-8984/21/23/233201.
83. Pasquale, M.; Sasso, C.P.; Lewis, L.H.; Giudici, L.; Lograsso, T.; Schlagel, D. Magnetostructural Transition and Magnetocaloric Effect in Ni55Mn20Ga25 Single Crystals. *Phys Rev B Condens Matter Mater Phys* **2005**, *72*, 094435, doi:10.1103/PHYSREVB.72.094435/FIGURES/5/MEDIUM.
84. Buchelnikov, V.D.; Sokolovskiy, V. V. Magnetocaloric Effect in Ni-Mn-X (X = Ga, In, Sn, Sb) Heusler Alloys. *The Physics of Metals and Metallography* **2012**, *112*, 633–665, doi:10.1134/S0031918X11070052.
85. Marcos, J.; Planes, A.; Mañosa, L.; Casanova, F.; Batlle, X.; Labarta, A.; Martínez, B. Magnetic Field Induced Entropy Change and Magnetoelasticity in Ni-Mn-Ga Alloys. *Phys Rev B* **2002**, *66*, 224413, doi:10.1103/PhysRevB.66.224413.
86. Krenke, T.; Duman, E.; Acet, M.; Wassermann, E.F.; Moya, X.; Manosa, L.; Planes, A. Inverse Magnetocaloric Effect in Ferromagnetic Ni–Mn–Sn Alloys. *Nature Materials* **2005**, *4*, 450–454, doi:10.1038/nmat1395.
87. Yuce, S.; Kavak, E.; Yildirim, O.; Bruno, N.M.; Emre, B. Investigation of the Inverse Magnetocaloric Effect with the Fraction Method. *Journal of Physics: Condensed Matter* **2023**, *35*, 345801, doi:10.1088/1361-648X/ACD3CE.
88. Kamantsev, A.P.; Koshkidko, Y.S.; Bykov, E.O.; Gottschall, T.; Gamzatov, A.G.; Aliev, A.M.; Varzaneh, A.G.; Kameli, P. Giant Irreversibility of the Inverse Magnetocaloric Effect in the Ni47Mn40Sn12.5Cu0.5 Heusler Alloy. *Appl Phys Lett* **2023**, *123*, 202405, doi:10.1063/5.0176772/2921289.
89. Gurunani, B.; Ghosh, S.; Gupta, D.C. Comprehensive Investigation of Half Heusler Alloy: Unveiling Structural, Electronic, Magnetic, Mechanical, Thermodynamic, and Transport Properties. *Intermetallics (Barking)* **2024**, *170*, 108311, doi:10.1016/J.INTERMET.2024.108311.
90. Lin, Z. Progress Review on Topological Properties of Heusler Materials., doi:10.1051/e3sconf/202021302016.
91. Moore, J.E. The Birth of Topological Insulators. *Nature 2010 464:7286* **2010**, *464*, 194–198, doi:10.1038/nature08916.
92. Rani, B.; Wani, A.F.; Sharopov, U.B.; Patra, L.; Singh, J.; Ali, A.M.; Abd El-Rehim, A.F.; Khandy, S.A.; Dhiman, S.; Kaur, K. Electronic Structure-, Phonon Spectrum-, and Effective Mass- Related Thermoelectric Properties of PdXSn (X = Zr, Hf) Half Heuslers. *Molecules 2022, Vol. 27, Page 6567* **2022**, *27*, 6567, doi:10.3390/MOLECULES27196567.
93. Jia, X.; Deng, Y.; Bao, X.; Yao, H.; Li, S.; Li, Z.; Chen, C.; Wang, X.; Mao, J.; Cao, F.; et al. Unsupervised Machine Learning for Discovery of Promising Half-Heusler Thermoelectric Materials. *npj Computational Materials 2022 8:1* **2022**, *8*, 1–9, doi:10.1038/s41524-022-00723-9.
94. Kumar, N.; Guin, S.N.; Manna, K.; Shekhar, C.; Felser, C. Topological Quantum Materials from the Viewpoint of Chemistry. *Chem Rev* **2021**, *121*, 2780–2815, doi:10.1021/ACS.CHEMREV.0C00732/ASSET/IMAGES/LARGE/CR0C00732_0028.JPEG.
95. Liu, Z.K.; Yang, L.X.; Wu, S.C.; Shekhar, C.; Jiang, J.; Yang, H.F.; Zhang, Y.; Mo, S.K.; Hussain, Z.; Yan, B.; et al. Observation of Unusual Topological Surface States in Half-Heusler Compounds LnPtBi (Ln=Lu, Y). *Nature Communications 2016 7:1* **2016**, *7*, 1–7, doi:10.1038/ncomms12924.
96. Tafti, F.F.; Fujii, T.; Juneau-Fecteau, A.; de Cotret, S.R.; Doiron-Leyraud, N.; Asamitsu, A.; Taillefer, L. Superconductivity in the Noncentrosymmetric Half-Heusler Compound LuPtBi : A Possible Topological Superconductor. *Phys Rev B Condens Matter Mater Phys* **2013**, *87*, doi:10.1103/PhysRevB.87.184504.
97. Butch, N.P.; Syers, P.; Kirshenbaum, K.; Hope, A.P.; Paglione, J. Superconductivity in the Topological Semimetal YPtBi. *Phys Rev B Condens Matter Mater Phys* **2011**, *84*, 220504, doi:10.1103/PHYSREVB.84.220504/FIGURES/4/MEDIUM.
98. Guo, P.-J.; Zhang, J.-F.; Yang, H.-C.; Liu, Z.-X.; Liu, K.; Lu, Z.-Y. LnPd$_{2}$Sn (Ln=Sc, Y, Lu) Class of Heusler Alloys for Topological Superconductivity. **2018**.
99. Joshi, V.K. Spintronics: A Contemporary Review of Emerging Electronics Devices. *Engineering Science and Technology, an International Journal***2016**, *19*, 1503–1513, doi:10.1016/J.JESTCH.2016.05.002.
100. Yakout, S.M. Spintronics: Future Technology for New Data Storage and Communication Devices. *J Supercond Nov Magn***2020**, *33*, 2557–2580, doi:10.1007/S10948-020-05545-8/TABLES/5.
101. Leclair, P.; Ha, J.K.; Swagten, H.J.M.; Kohlhepp, J.T.; Van De Vin, C.H.; De Jonge, W.J.M. Large Magnetoresistance Using Hybrid Spin Filter Devices. *Appl Phys Lett***2002**, *80*, 625–627, doi:10.1063/1.1436284.
102. Herran, J.; Carlile, R.; Kharel, P.; Lukashev, P. V. Half-Metallicity in CrAl-Terminated Co2CrAl Thin Film. *J Phys Condens Matter***2019**, *31*, doi:10.1088/1361-648X/AB3D6C.

103. Jourdan, M.; Minár, J.; Braun, J.; Kronenberg, A.; Chadov, S.; Balke, B.; Gloskovskii, A.; Kolbe, M.; Elmers, H.J.; Schönhense, G.; et al. Direct Observation of Half-Metallicity in the Heusler Compound Co2MnSi. *Nature Communications* **2014**, *5*, 1–5, doi:10.1038/ncomms4974.
104. Kc, S.; Mahat, R.; Regmi, S.; Mukherjee, A.; Padhan, P.; Datta, R.; Butler, W.H.; Gupta, A.; Leclair, P. Tunable Properties and Potential Half-Metallicity in (Co_{2−x}Ti_{x})FeGe Heusler Alloys: An Experimental and Theoretical Investigation Tunable Properties and Potential Half-Metallicity in (Co 2−x Ti x)FeGe Heusler Alloys: An Experimental and Theoretical Investigation. *Phys. Rev. Materials* **2019**, *3*, 114406, doi:10.1103/PhysRevMaterials.3.114406.
105. Inomata, K.; Ikeda, N.; Tezuka, N.; Goto, R.; Sugimoto, S.; Wojcik, M.; Jedryka, E. Highly Spin-Polarized Materials and Devices for Spintronics∗. *Sci Technol Adv Mater* **2008**, *9*, 14101, doi:10.1088/1468-6996/9/1/014101.